

ELECTRICAL PROPERTIES OF A CARBON NANOTUBE/POLYMER NANOCOMPOSITE AND ITS APPLICATION AS HIGHLY SENSITIVE STRAIN SENSORS

Ning Hu¹, Zen Masuda and Hisao Fukunaga

Department of Aerospace Engineering, Tohoku University,
Aramaki-Aza-Aoba 6-6-01, Aoba-ku, Sendai 980-8579, Japan

ABSTRACT

Carbon nanotubes (CNTs) of high aspect ratio possess excellent electrical conductivity. Therefore, with a little amount of CNTs, which are dispersed into insulating polymers, it is possible to manufacture CNT/polymer nanocomposites with very high electrical conductivity. This kind of conductive nanocomposites can be employed in various applications, such as highly sensitive strain sensors and electromagnetic interference materials.

In this Chapter, we will mainly describe our research outcomes about the electrical properties of CNT/polymer nanocomposites from experimental and theoretical studies. First, in this work, based on the statistical percolation theory, we proposed a three dimensional (3D) numerical model to predict the electrical properties of a nanocomposite made from an insulating polymer with filled CNTs. In this model, with the assumption of randomly distributed CNTs in the polymer, the percolation threshold was estimated at the volume fraction of CNTs when the first complete electrically-conductive path connected by some CNTs is formed. Furthermore, to predict the electrical conductivity of the nanocomposite after the percolation threshold, a 3D resistor network model was constructed, in which Kirchhoff's current law was adopted to set up the system algebraic equations at different nodes in the network formed by CNTs. The macroscopic current of the nanocomposite under the applied external voltage was calculated by solving these equations, and then Ohm's law was employed to predict the macroscopic electrical conductivity of the nanocomposite. The influences of curved shapes of CNTs, aggregates

¹ To whom all correspondence should be addressed: Email: hu@ssl.mech.tohoku.ac.jp (Ning Hu) Fax: +81-22-795-4109.

of CNTs and tunnel effect among CNTs on the percolation threshold and the electrical conductivity have been investigated in detail.

To verify the above numerical model, a lot of experiments have also been performed by the authors. The effects of various factors in the in situ polymerization fabrication process on the electrical performances of the nanocomposite were explored. The present experimental results plus some previous experimental results by other researchers were found to agree with the present numerical results very well. Moreover, a simple yet reliable empirical percolation theory has been obtained based on the detailed numerical investigations.

For the application of this nanocomposite as highly sensitive strain sensors, by considering the tunnel effect among CNTs and the rigid-body movement of CNTs in the polymer caused by the prescribed strain, the above numerical model was further extended for modeling the electrical resistance change of the nanocomposite due to the strain. The relation between the applied strain and the electrical resistance change was estimated numerically and measured experimentally. Both numerical and experimental results, which are in very good agreement, demonstrate that the CNT/polymer sensors possess much higher sensitivity or gauge ratio compared with the traditional strain gauge. The tunnel effect was found to be a key factor to control the performance of this new-type strain sensor.

Keywords: *carbon nanotube; polymer; electrical property; nanocomposites; statistical percolation model*

1. INTRODUCTION

Recently, much attention has been paid to the fabrication of nanocomposites with the use of carbon nanotubes (CNTs) in polymer materials to harness the exceptional intrinsic properties of CNTs. In particular, polymers with the incorporation of CNTs show great potential for electronic device applications, such as organic field emitting displays, photovoltaic cells, highly sensitive strain sensors, electromagnetic interference materials, etc. Generally, for the different applications, the different electrical properties of nanocomposites are employed. For instance, for the application of strain sensors, direct current (DC) properties of nanocomposites are needed. Meanwhile, for the application of electromagnetic interference materials, alternate current (AC) properties of nanocomposites are needed. In the recent decade, numerous experimental studies on the electrical properties of nanocomposites made from insulating polymers filled by CNTs have been carried out [1-19].

In this work, we will focus on the DC properties of nanocomposites. To prepare this kind of nanocomposites, currently, melt mixing compounding [1-4], curing/in situ polymerization [5-17] and coagulation [18, 19] are widely used. Depending on the polymer matrix and processing technology as well as the type of nanotube material used, percolation thresholds ranging from less than 1.0 wt% to over 10.0 wt% of CNTs loading have been observed experimentally [12]. For example, for single-wall carbon nanotubes (SWNTs), Nogales *et al.* [5] applied in situ polycondensation reaction to prepare SWNT/PBT nanocomposites and achieved an electrical percolation threshold as low as 0.2 wt% of SWNTs loading. Ounaies *et al.* [6] have investigated the electrical properties of SWNTs reinforced polyimide (CP2) composites. The obtained conductivity obeys a percolation-like power law with a low

percolation threshold of around 0.1 wt%. The bundling phenomenon of SWNTs within the matrix has been identified in experimental analysis. Park *et al.* [7] have shown that it is possible to control the electrical properties of SWNT/polymer composites through the techniques of alignments of SWNTs. Kymakis *et al.* [8] studied the electrical properties of SWNTs filled in the soluble polymer poly(3-octylthiophene) (P3OT). The reported percolation threshold is around 11 wt%. In their latter work [9], purified SWNTs were used, which lead to a much lower percolation threshold at around 4 wt%.

For multi-wall carbon nanotubes (MWNTs), Sandler [10] have employed MWNTs with an epoxy polymer based on bisphenol-A resin and an aromatic hardener, and they got a lower percolation threshold at around 0.04 wt%. The formation of aggregates was also identified. Sandler *et al.* [11] reported the lowest percolation threshold up to the present date, i.e., 0.0025 wt% using MWNTs. To obtain a low percolation threshold, using MWNTs and epoxy, Martin *et al.* [12] investigated the influence of process parameters employed in the in situ polymerization fabrication process, such as stirring rate, resin temperatures and curing temperatures. It was found that the electrical properties of nanocomposites strongly depend on the choice of these parameters. Using the in situ polymerization process, the MWNT/polymer nanocomposites were prepared in [13-15], and the obtained percolation thresholds were found to be lower than 1.0 wt%. Hu *et al.* [19] prepared the MWNT/PET nanocomposites by means of coagulation process. Uniform dispersion of MWNTs throughout PET matrix was confirmed by transmission electron microscopy (TEM) and scanning electron microscopy (SEM). The obtained percolation threshold is around 0.9 wt%.

Generally, there are two issues addressed in many previous studies: dispersion of CNTs in polymer matrix and interaction between CNTs and polymer. For the first issue, due to the high surface-to-mass ratio of CNTs, molecular scale forces and interactions should be considered among CNTs. Van der Waals forces usually promote flocculation of CNTs, whilst electrostatic charges or steric effects lead to a stabilization of the dispersion through repulsive forces [6, 12]. As a consequence, by considering the nature of percolating network formed by very fine filler, e.g., CNTs, the balance of the two factors of reverse effects outlined above should be taken into account. For the second issue, the fact, that the nanotubes in the composites are coated or encapsulated by a thin insulating polymer layer, was identified for SWNTs [9] and MWNTs [19]. This encapsulation acts as a barrier to the electrical charge transfer between nanotubes [9].

As mentioned above, although a lot of experimental studies have been performed recently, whereas, except the study in [12], there is little literature covering the detailed influences of various factors in the fabrication process on the electrical properties of CNT/polymer nanocomposites using in situ polymerization method to our knowledge. Moreover, there has been almost no systematically theoretical or numerical work for comprehensively understanding the electrical characteristics of the nanocomposites at and after the percolation threshold except that the percolation threshold was determined by a numerical model [6] with randomly distributed CNTs in a polymer and by an empirical formula from the extruded volume approach based on the statistical percolation theory [12].

Generally, by gradually filling some traditional conductive filler particles, such as carbon short fibers, into insulating polymers, the variation of electrical conductivity of composites can be divided into three stages as shown in Figures 1.1 and 1.2. In the first stage, the electrical conductivity is very low since there are few filler particles in matrix as shown in Figure 1.1(a) and Figure 1.1(b). In Figure 1.1(b), some large clusters connected by fillers are

gradually formed. In this first stage, the electrical conductivity of composites is close to that of the polymer as shown in Figure 1.2. In the second stage, as the amount of filler particles increases, the first complete electrically-conductive path connected by some filler particles is formed as shown in Figure 1.1(c). In this second stage, the electrical conductivity will increase remarkably following a percolation power law as shown in Figure 1.2. This process is called as percolation process. The volume fraction of filler particles at this stage is called as the percolation threshold, i.e., ϕ_c . In the final stage, with the further addition of filler particles into the polymer, a lot of electrically-conductive paths, which forms a conductive network, can be constructed as shown in Figure 1.1(d), and the electrical conductivity further increases gradually, until leveling off at a constant, which is close to that of the element or filler of conductive network in Figure 1.2. From the previously published experimental results, it was found that the electrical behavior of nanocomposites using CNTs as conductive filler particles in polymer matrix follows the same percolation phenomenon. For some traditional electronic composites with fillers [20-22], e.g. carbon short fibers or carbon flakes, there have been some theoretical or numerical studies based on the traditional statistical percolation model, especially for predictions of percolation threshold. *It is therefore natural to ask if the statistical percolation model is still valid to describe the electrical behaviors of the nanocomposites with such a fine filler, as CNTs.*

In this study, for an insulating polymer with random distributed CNTs, first, based on the statistical percolation model, we developed a three dimensional (3D) numerical model with two stages for investigating the electrical properties of nanocomposites at and after the percolation threshold. In the first stage, the percolation threshold was predicted at the volume fraction of CNTs when the first complete electrically-conductive path connected by some CNTs is formed in matrix. In the second stage, a 3D resistor network model was constructed to predict the macroscopic electrical conductivity of nanocomposites after the percolation threshold. This model demonstrates remarkable success in capturing the main features of electrical behaviors of nanocomposites. The influences of various factors, such as the curved shapes of CNTs, the aggregates of CNTs in matrix and tunnel effect among CNTs on the electrical properties of nanocomposites have been studied. Then, the verified numerical model was employed to construct a simple and reliable empirical percolation theory.

Next, we experimentally investigated the electrical properties of MWNT/polymer nanocomposites. The specimens were prepared by in situ polymerization method. For the case of 2 wt% of MWNTs loading, the effects of various factors in the fabrication process on the electrical behaviors of the nanocomposites have been studied. It was found that the bulk conductivity of the nanocomposites is significantly sensitive to some factors in the fabrication process, such as curing temperature and mixing process. The experimental results plus some other previous experimental results have been employed to validate the proposed numerical model.

Finally, the currently fabricated MWNT/polymer nanocomposites have been applied as highly sensitive sensors. Moreover, by considering the tunnel effect, the present numerical model was further extended into the case of nanocomposites with prescribed strains. The relation between the strain and the electrical conductivity was estimated numerically and experimentally. Finally, both numerical and experimental results demonstrate that this new-type sensor possesses much higher sensitivity or gauge ratio compared with the traditional

strain gauge. Moreover, it was found that the tunnel effect among CNTs plays a key role in determining the performance of this new-type sensor.

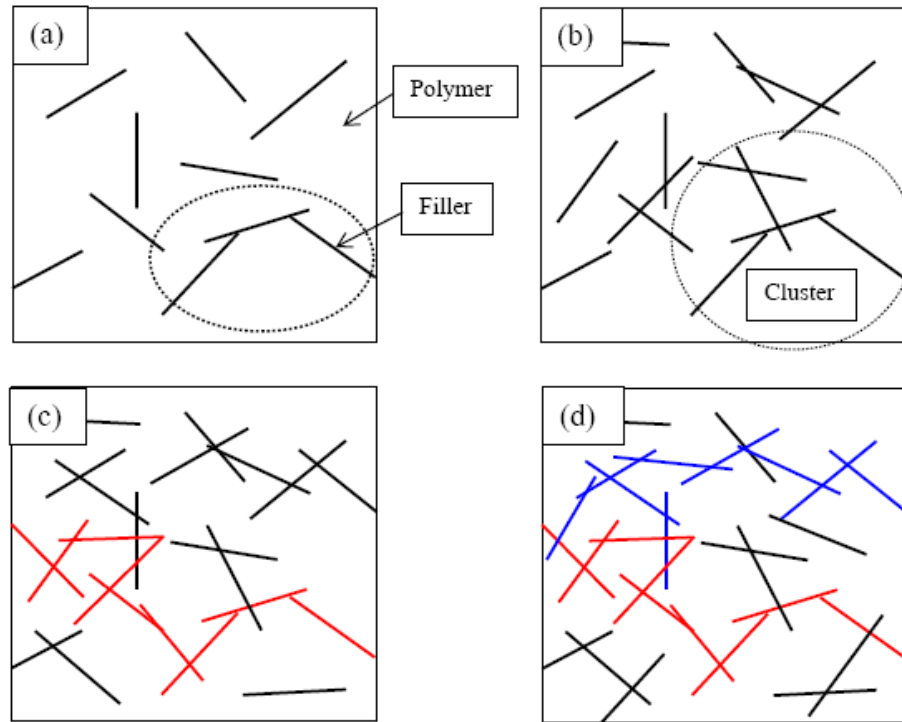


Figure 1.1 Percolation process in electronic composites

2. A STATISTICAL PERCOLATION MODEL FOR PREDICTION OF PERCOLATION THRESHOLD OF NANOCOMPOSITES

In this section, we will mainly describe several key steps to create a statistical numerical model for predicting the percolation threshold of nanocomposites based on the assumption of that CNTs are randomly distributed in a polymer. First, we will show how to generate this numerical model with the different features what we need. Second, we will employ the generated model as well as a powerful algorithm to find the value of percolation threshold. Finally, this model will be used to obtain the percolation threshold and to investigate the influences of various factors.

2.1. Generation of Model of Randomly Distributed CNTs in Matrix

First, as shown in Figure 2.1, we consider a 3D representative unit element, which is only a small and local portion of the whole nanocomposite body. However, there are enough CNTs contained in this 3D element, which can effectively represent the macroscopic and bulk

electrical properties of nanocomposites. Our goal is to find the volume fraction or weight fraction of CNTs when the first complete conductive path is formed by some CNTs, e.g. from the left side to the right side of the 3D cube in Figure 2.1. Three cases which may be possibly encountered in the practical nanocomposites are considered in this research. This first one is a model with the uniform random distribution of straight CNTs, which is a simplest model for the ideal dispersion of CNTs in matrix. The second one is a model in which the shape of practical CNTs is considered, e.g., the curved CNTs considered here. The third one relates to the fabrication process of nanocomposites, where the perfect dispersion cannot be realized practically. Therefore, in this model, the aggregates of CNTs are modeled. We will introduce these models one by one and state the main steps to construct them.

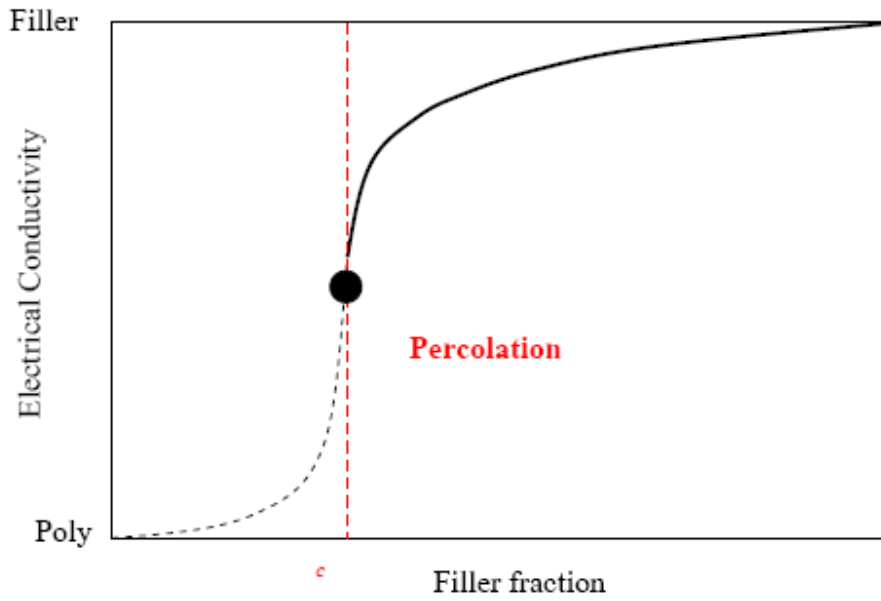


Figure 1.2. Electrical conductivity of electronic composites as a function of filler fraction.

2.1.1. Model of Uniform Random Distribution of Straight CNTs

In this study, to predict the percolation threshold of this nanocomposite numerically, as shown in Figure 2.1, we consider a 3D element with uniform random distribution of straight CNTs. The so-called ‘soft-core’ CNTs of the length of L and the diameter of D are considered as capped cylinders, which are allowed to penetrate each other. This assumption can lead to the tremendous reduction in the computational cost, which results in a proper solution method suitable for the Monte-Carlo procedure used here. The capped cylinders are randomly put in the 3D cube and their orientations in space are chosen randomly. This procedure for numerical prediction of percolation threshold is similar in principle to the ones in [6, 22]. For this ideal state of uniformly dispersed straight CNTs in matrix, the following method can be employed.

The coordinates of two ends of a CNT, i.e. (x_1, y_1, z_1) and (x_2, y_2, z_2) can be set as

$$x_1 = rand \times L_x \quad (1a)$$

$$y_1 = rand \times L_y \quad (1b)$$

$$z_1 = rand \times L_z \quad (1c)$$

$$x_2 = x_1 + L \cdot v_1 \cdot \cos(w_1) \quad (1d)$$

$$y_2 = y_1 + L \cdot v_1 \cdot \sin(w_1) \quad (1e)$$

$$z_2 = z_1 + L \cdot u_1 \quad (1f)$$

where as shown in Figure 2.1, L_x , L_y and L_z are the lengths of the 3D element along x , y and z axes, respectively, and *rand* is a random number located in $[0,1)$, which is uniformly generated. Also, the alignment directions of CNTs, i.e., u_1 , v_1 and w_1 are expressed as follows

$$u_1 = 1.0 - 2.0 \times rand \quad (2a)$$

$$v_1 = \sqrt{1.0 - u_1^2} \quad (2b)$$

$$w_1 = 2\pi \times rand \quad (2c)$$

2.1.2. Model of Uniform Random Distribution of Curved CNTs

As shown in Figure 2.2 from our SEM observation for a specimen of 13 wt.% MWNTs loading, practically, CNTs are not perfectly straight. To model this curved shape of CNTs, a very simple method is proposed in this study. First, as shown in Figure 2.2, we divide each CNT into several segments (10 segments are used in this research). The angle in 3D space between arbitrary two adjacent segments can randomly vary within a circular cone with a top angle θ_{max} . For the divided CNTs, the coordinates of the first end, i.e., x_1 , y_1 and z_1 , can be determined using Eqs (1a)-(1c), and the coordinates of the subsequent points can be determined as follows one by one

$$x_{i+1} = x_i + L \cdot v_{i+1} \cdot \cos(w_{i+1})/N \quad i = 1, N \quad (3f)$$

$$y_{i+1} = y_i + L \cdot v_{i+1} \cdot \sin(w_{i+1})/N \quad i = 1, N \quad (3g)$$

$$z_{i+1} = z_i + L \cdot u_{i+1}/N \quad i = 1, N \quad (3h)$$

where

$$w_{i+1} = w_i \pm \theta_{max} \times rand \quad i = 1, N \quad (3c)$$

$$u_{i+1} = \sin \left\{ \tan^{-1} \left(\frac{u_i}{v_i} \right) + \tan^{-1} \left(\frac{u'}{v'} \right) \right\} \quad i = 1, N \quad (3d)$$

$$v_{i+1} = \cos \left\{ \tan^{-1} \left(\frac{u_i}{v_i} \right) + \tan^{-1} \left(\frac{u'}{v'} \right) \right\} \quad i = 1, N \quad (3e)$$

where

$$u' = \sin(\theta_{max}) \cdot (1.0 - 2.0 \times rand) \quad (3a)$$

$$v' = \sqrt{1.0 - u'^2} \quad (3b)$$

where θ_{max} is the angle of the cone top, N is the number of divisions. Also, u_1 , v_1 and w_1 are determined using Eqs (2a)-(2c).

2.1.3. Model of Aggregates of Straight CNTs

Usually, due to the high surface-to-mass ratio of CNTs resulting in strong absorption energies among CNTs, there are some aggregates or bundling formed by CNTs caused by a poor dispersion process. Especially, for SWNTs, due to their much smaller sizes compared with those of MWNTs, this phenomenon may be more obvious. To generate these aggregates numerically, the well-known Box-Muller method using two random numbers is employed. The aggregates of CNTs with normal distribution are artificially created in matrix. This method is briefly described here. First, the coordinates of the starting point of a CNT, i.e., x_1 , y_1 and z_1 , are determined as

$$x_1 = L_{xc} + L_x \mu \sqrt{-2 \log(U_{x1}/L_x)} \cdot \cos(2\pi U_{x2}/L_x) \quad (4a)$$

$$y_1 = L_{yc} + L_y \mu \sqrt{-2 \log(U_{y1}/L_y)} \cdot \cos(2\pi U_{y2}/L_y) \quad (4b)$$

$$z_1 = L_{zc} + L_z \mu \sqrt{-2 \log(U_{z1}/L_z)} \cdot \cos(2\pi U_{z2}/L_z) \quad (4c)$$

where L_{xc} , L_{yc} and L_{zc} are the coordinates of the center of an aggregate, respectively, and μ is a parameter to determine the extensity of the aggregate with normal distribution. A higher μ means the larger volume of the aggregate with lower density of CNTs, and

$$U_{x1} = rand \times L_x \quad U_{x2} = rand \times L_x \quad (5a)$$

$$U_{y1} = rand \times L_y \quad U_{y2} = rand \times L_y \quad (5b)$$

$$U_{z1} = rand \times L_z \quad U_{z2} = rand \times L_z \quad (5c)$$

In our analysis, for the sake of simplicity, only four aggregates are modeled in the 3D representative element, and the coordinates of their centers are $(L_x/4, L_y/4, L_z/2)$, $(L_x 3/4, L_y/4, L_z/2)$, $(L_x/4, L_y 3/4, L_z/2)$ and $(L_x 3/4, L_y 3/4, L_z/2)$, respectively.

After obtaining the coordinates of the starting end of the CNT in Eqs (4), for the coordinates of another end of the CNT, Eqs (1d)-(1f) and (2a)-(2b) can be simply applied. Naturally, this model is not a practical one, for example, due to the small number of aggregates modeled here, the isotropy of electrical properties of the 3D element cannot be guaranteed. However, we can still employ it to qualitatively investigate the influences of aggregates on the electrical properties of nanocomposites.

2.1.4. Judgment of Contact Between CNTs

In our numerical model, CNTs are randomly put into the 3D cube one by one. It is a key step to judge if the dispersed CNTs are in the state of contact, which may lead to the formation of possible conductive clusters as shown in Figure 1.1(b). To determine if the generated CNTs using the techniques outlined in the above section are in the state of contact, we consider three possible contacting patterns between two CNTs shown in Figure 2.3.

For the case of Figure 2.3(a), from the coordinates of two ends of CNT1 and CNT2, we can calculate the distance between CNT1 and CNT2. First, we consider the differences of three coordinates of two ends of CNT1 and CNT2 as follows: $(x_1, y_1, z_1) - (x_2, y_2, z_2)$ and $(x_3, y_3, z_3) - (x_4, y_4, z_4)$. Then, the vectors of alignment directions of CNT1 and CNT2, i.e., d_1 and d_2 are determined as follows

$$d_1 = (x_2 - x_1, y_2 - y_1, z_2 - z_1) \quad (6a)$$

$$d_2 = (x_4 - x_3, y_4 - y_3, z_4 - z_3) \quad (6b)$$

Also, we define the difference of coordinates of the starting ends of CNT1 and CNT2 as follows

$$p_1 - p_3 = (x_1 - x_3, y_1 - y_3, z_1 - z_3) \quad (7)$$

Then, by using Eqs. (6a)-(6b) and Eq. (7), the shortest distance d between CNT1 and CNT2 can be evaluated as follows

$$d = \frac{\|p_1 - p_3, d_1 \times d_2\|}{\|d_1 \times d_2\|} \quad (8)$$

Next, for the contacting pattern shown in Figure 2.3(b), the shortest distance d between CNT1 and CNT2 at the point 3 can be simply calculated as follows

$$d = \frac{\|a \times d_1\|}{\|d_1\|} \quad (9)$$

where $a = (x_3 - x_2, y_3 - y_2, z_3 - z_2)$, and d_1 is evaluated by Eq. (6a).

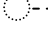
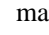
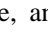
Finally, for the contacting pattern shown in Figure 2.3(c), the shortest distance d between CNT1 and CNT2 at the point 3 can be simply calculated as

$$d = \sqrt{(x_1 - x_3)^2 + (y_1 - y_3)^2 + (z_1 - z_3)^2} \quad (10)$$

When the estimated distance between two CNTs is lower than the diameter of CNTs, it can be thought of that two CNTs are in the state of contact. Note that in our numerical model, the ‘soft-core’ CNTs are used, which are allowed to penetrate each other. Therefore, in our numerical model, there may be overlapping among CNTs to a certain extent. However, when the volume fraction of CNTs is low and the aspect ratio of CNTs is large, the error caused by this overlapping is negligible.

2.1.5. Union/Find Algorithm for Searching for Cluster Formation

The tree-based union/find algorithm [23] was adopted to detect the first complete conductive path connecting two sides of 3D cube (as red CNTs marked in Figure 2.1), and then the percolation threshold can be determined using the total volume of CNTs at this point. This algorithm is very quick, which is suitable for a Monte-Carlo procedure used here.

When two CNTs are in the state of contact, a cluster can be formed. As the amount of filled CNTs in matrix increases, the number of CNTs, which are in the state of contact, will also increase, which results in some larger clusters gradually as shown in Figure 1.1(b). With the further addition of CNTs in matrix up to a critical volume fraction, one of the clusters will connects the two sides of the 3D element, which finally forms the first complete conductive path or network within the 3D element. At this point, the electrical conductivity of nanocomposites will remarkably increase and the volume fraction of CNTs can be thought of as the percolation threshold what we need. Generally, with the addition of one cylinder (here, a CNT) into matrix, to search for if two clusters are amalgamated, the tree-based union/find algorithm can be adopted, which was proposed by Newman *et al.* [23] for the percolation problem in a square lattice. In this research, we just extend this algorithm to the case of the 3D element with randomly distributed CNTs, as schematically shown in Figure 2.4. In Figure 2.4(a),  represents a newly added CNT into matrix. In Figure 2.4(b), the sequence number of happening of CNTs is labeled. Also,  marks the ‘child’ of a tree, and  represents the ‘root’ site of the tree.

The basic steps involved in the union/find algorithm are briefly stated as follows

- i) As shown in Figure 2.4(a), each CNT without contact with other clusters is considered to be an independent 'root' site of a tree or a cluster in matrix, respectively, e.g., CNT2 in Figure 2.4(b).
- ii) For a 3D element with sizes of L_x , L_y and L_z , one CNT is randomly added into it.
- iii) For the added CNT, its root is recorded to be a cluster of size of 1. Also, the happening number of this CNT is labeled and its maximum and minimum x coordinates, i.e., the x coordinates at two ends are recorded.
- iv) For the newly added CNT in step (ii), the judgment of contact state between it and other CNTs is performed. If there is no contact, return to (ii) (for instance for CNT1 and CNT2 in Figure 2.4(b)). If there is only one contacting point, the root of the cluster contacted by the newly added CNT is searched for (e.g. CNT8 and CNT10). If there are more than one contacting points, such as two contacting points, the roots of two clusters connected by this CNT (e.g. CNT12) are searched for. At this point, the roots are searched by following the pointers shown in Figure 2.4(b).
- v) For the case of one contacting point outlined in (iv), the size of the pre-existing cluster should be at least equal to or larger than that of the newly added CNT of the size of 1, the size of this cluster is increased by 1 and the root of the added CNT is relabeled as that of the cluster. For the case of two or more contacting points, e.g. two contacting points here, if the roots of two clusters connected by the added CNT are the same one, the root of the added CNT is relabeled as it. The size of this cluster is increased by 1.
- vi) If the roots of two clusters are different, the comparison of the sizes of two clusters is performed. The root of the cluster with a smaller size should be relabeled as the root of the cluster with a larger size (e.g., see CNT5 and CNT7 in Figure 2.4(b)). The root of the added CNT is also relabeled as the one of the cluster with the larger size. The size of the cluster should be also changed into that of the final amalgamated one.
- vii) If the maximum and minimum x coordinates of the cluster formed at steps (v) or (vi) change, the new data about cluster coordinates should be recorded as well as the root site.
- viii) If the maximum x coordinate of the cluster formed at steps (v) or (vi) achieves at L_x , and the minimum x coordinate of the cluster is equal to 0. At this point, the total volume of all CNTs is calculated. Otherwise, return to the step (ii). The volume V_{CNT} of all CNTs of the number of M is expressed as follows

$$V_{CNT} = \left(\frac{1}{6} \pi D^3 + \frac{1}{4} \pi D^2 L \right) M \quad (11)$$

The total volume of CNTs obtained in (viii) is used to predict the percolation threshold, ϕ_p (vol%) as follows

$$\phi_p = \frac{V_{CNT}}{L_x \cdot L_y \cdot L_z} \times 100 \quad (12)$$

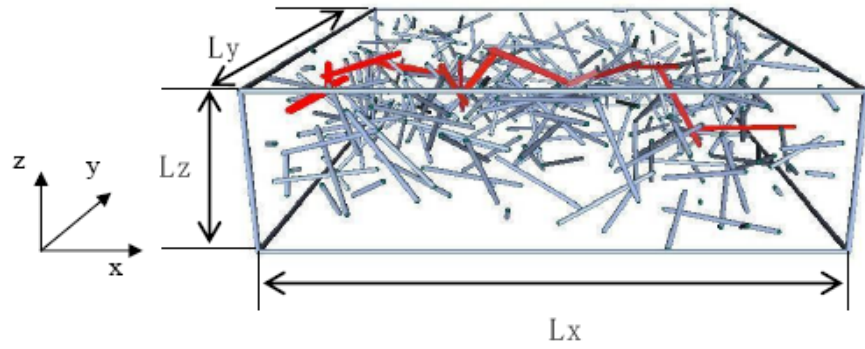


Figure 2.1. Schematic view of a representative 3D element with randomly dispersed CNTs.

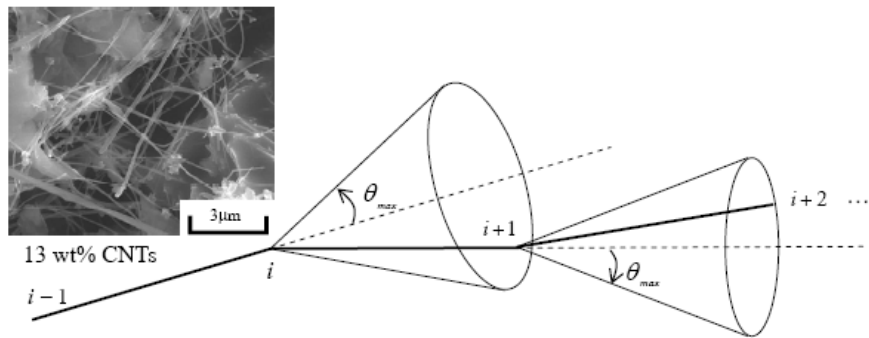


Figure 2.2. Definition of divided segments of CNTs for modeling curved CNTs.

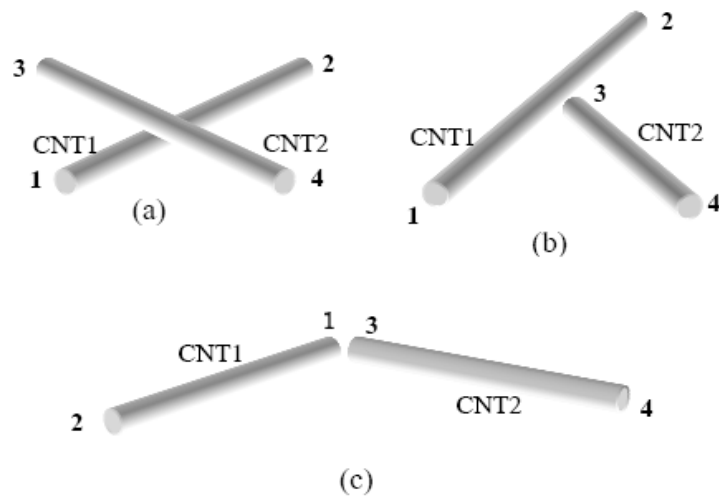


Figure 2.3. Contact between two CNTs: (a) skew of CNT1 and CNT2; (b) CNT1 and node 3 of CNT2; (c) node 1 of CNT1 and node 3 of CNT2.

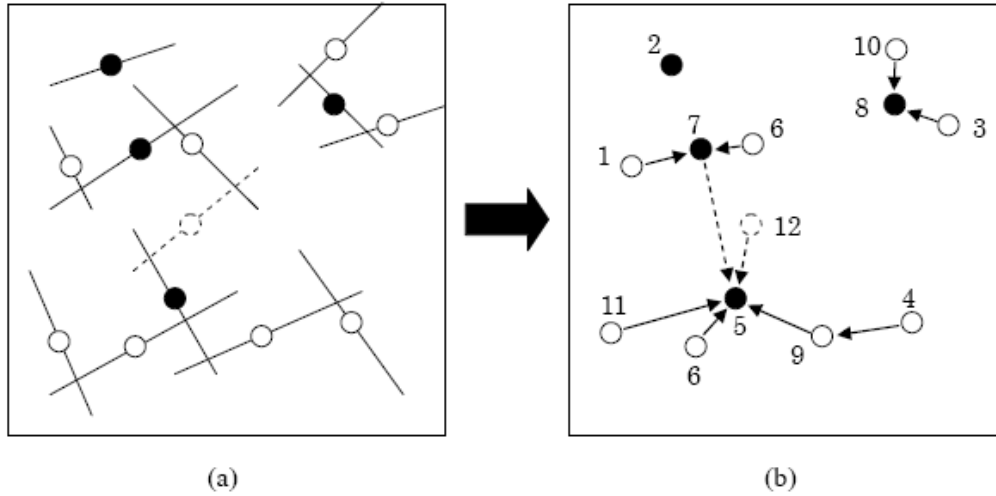


Figure 2.4. An example of the tree structure for CNT fillers.

2.2. Numerical Results of Percolation Threshold and Investigations

In this section, we will focus on the numerical investigation of percolation threshold using the statistical percolation model outlined previously. The influences of various factors, such as the shapes and aggregates of CNTs will be explored.

Determination of Sizes of Representative 3D Element

Before entering into the stage of the detailed investigations, to determine the sizes of the representative 3D cube, which can represent the macroscopic and bulk electrical properties of nanocomposites, the following two aspects have to be considered.

The first one is about the anisotropy of percolation threshold. It means that the electrical properties along three axis directions of 3D cube in Figure 2.1 should be approximately the same to guarantee the bulk electrical properties to be correct. We have calculated the percolation thresholds along three axis directions of the 3D cube. As shown in Figure 2.5(a), we can find that for the case of $L_x/L=L_y/L=L_z/L=1$, there is obvious anisotropy along different directions. However, when $L_x/L \geq 2$, $L_y/L \geq 2$ and $L_z/L \geq 2$, the anisotropic characteristic of percolation threshold is negligible. The percolation thresholds along three axis directions are almost identical.

The second one is about the convergence of results. For the aspect ratio (L/D) of 100, Figure 2.5(b) shows that the sizes of $L_x/L=L_y/L=5$ and $L_z/L=2.0$ of the 3D cube can yield sufficiently stable results. Moreover, Figure 2.5(c) illustrates the percolation thresholds at the different simulation runs in our Monte-Carlo procedure. Again, $L_x/L=5$ and $L_z/L=2.0$ can generate the converging results with very small standard deviation. The percolation thresholds generated at the different random simulation runs are almost constant.

By considering the isotropy and convergence of results, the sizes, i.e., $L_x/L=L_y/L=5$ and $L_z/L=2.0$, were used consistently later. By fixing the length of CNTs, we adjust the diameter of CNTs to achieve the different values of aspect ratios of CNTs. We have also provided the results of a 2D model in Figure 2.5(b). From it, it can be found that the results of the 2D

model are quite higher than the converging results of the 3D model. It means that a 2D model may be improper for this kind of simulations. Finally, a Monte-Carlo procedure of 100 simulations has been performed to obtain the average percolation threshold at each volume fraction of CNTs.

Percolation Threshold of Straight CNTs

First, for the uniform random distribution of straight CNTs, the results of percolation threshold versus the aspect ratio of CNTs are shown in Figure 2.6. In fact, for the traditional statistical percolation theory, it is well-known that the percolation threshold strongly depends on the aspect ratio of filler. The results estimated from an empirical statistical percolation theory (excluded volume approach [20]) are also plotted in this figure for comparison. From Figure 2.6, we can find that our numerical results agree with the theoretical ones [20] very well although the slopes of two kinds of results are slightly different, which may be caused by some simplifications in the empirical statistical percolation formula.

By using the numerically obtained results and the least-square fitting, we can obtain the percolation threshold ϕ_c for straight CNTs with uniform random distribution in matrix as follows

$$\phi_c = \left(\frac{L}{D} \right)^{-1.1 \pm 0.03} \quad (13)$$

This formula is of much simpler form compared with some traditional empirical theories, e.g. [20], from which the percolation threshold can be estimated effectively based on the aspect ratio of CNTs only.

Naturally, it should be noted that this formula is obtained by fitting the results of numerical simulations for the filler of high aspect ratio, at least larger than 10 from our numerical experiences. For the cases of lower aspect ratio, this formula is invalid.

2.2.3. Influences of Shapes and Aggregates of CNTs on Percolation Threshold

Next, we will investigate the influences of shapes and aggregates of CNTs on the percolation threshold of nanocomposites. First, for curved CNTs, when θ_{max} defined in Figure 2.2 is equal to 15° , 30° , 45° and 60° , respectively, the configurations of the 3D element containing curved CNTs are shown in Figure 2.7. From it, we can see that as θ_{max} increases, the CNTs are more curved. Also, we can find that the curved CNTs can be modeled properly using the proposed technique. In these models, the number of divisions of CNTs is fixed to be 10. Figure 2.8 demonstrates the influence of θ_{max} on the percolation threshold when the aspect ratio of CNTs is taken as 100. In this figure, $\theta_{max} = 0$ represents straight CNTs. From this figure, it can be found that as θ_{max} increases, the percolation threshold increases gradually. This result is intuitively reasonable. If we consider a simple conductive path, which is from the left side to the right side of the 3D cube, it is more difficult to form this path using the curved CNTs due to their projected lengths in the horizontal plane (x - y plane in Figure 2.1) are shorter compared with those of straight CNTs. Moreover, the effect of θ_{max}

on the percolation threshold seems to be quite stable, and the percolation threshold changes continuously with the variation of θ_{max} .

Another important factor, which may influence the electrical properties of nanocomposites significantly, is aggregation of CNTs. Although as shown later in our SEM observations, we have not identified the obvious aggregates in our experimental specimens when using MWNTs, this factor is still important for modeling these nanocomposites since there may be aggregates or bundling of CNTs caused by the improper dispersion process as reported in many previously studies [6], especially for SWNTs. As shown previously, we employ the well-known Box-Muller method to form the aggregates with gathered CNTs of normal distribution. For the sake of simplicity, only four aggregates in our model are considered. The generated aggregation models of CNTs are schematically shown in Figure 2.9. To qualitatively investigate this problem, we define the following parameter:

$$\delta = \frac{V_{agg}}{V_{1/4}} \quad (14)$$

where V_{agg} is the approximate volume of a sphere containing one aggregate, and $V_{1/4}$ is one quarter of the total volume of the 3D element shown in Figure 2.9(a).

Therefore, δ can approximately and qualitatively describe the extensity of aggregates although it is not so strict. For different values of δ in Figure 2.9, we can find that as δ increases, the aggregates extend more widely, but with the lower density of CNTs included in them. The influence of aggregates on the percolation threshold is shown in Figure 2.10. From it, we can find that heavily concentrated aggregates may lead to very high percolation thresholds. However, when δ is larger than a critical value, i.e. 0.05 in our model, the aggregates have no obvious influence on the percolation threshold of nanocomposites. It means that, unless there are heavily concentrated aggregates corresponding to a very small value of δ , the influence of aggregates on the percolation threshold is almost ignorable. Naturally, it should be noted again that this investigation is only of the qualitative meaning, not quantitative one. However, it does tell us how important to avoid the heavily concentrated aggregates of CNTs through a proper dispersion process when fabricating this nanocomposite. Also, from Figure 2.10, it can found that when δ ranges from 0.1 to 0.6, the percolation threshold decreases slightly with δ decreases, which implies that relatively mild aggregates may be beneficial to the formation of conductive network. Therefore, for the different types of aggregates, such as mild aggregates or chain-like aggregates of CNTs discussed in our experimental investigations, the influence of aggregates might be different.

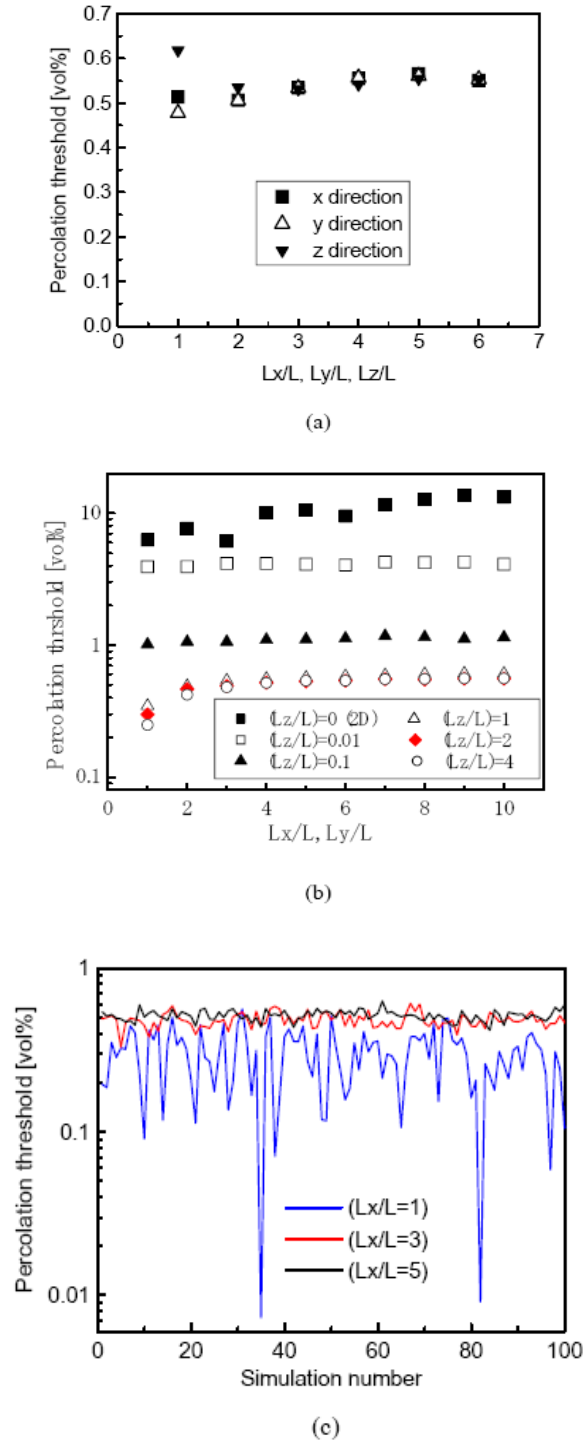


Figure 2.5. Verification of isotropy and convergence of representative element: (a) Percolation thresholds along x, y and z directions; (b) Size dependence of percolation threshold ($L/D=100$); (c) Percolation threshold versus simulation number for $L_z/L = 2$

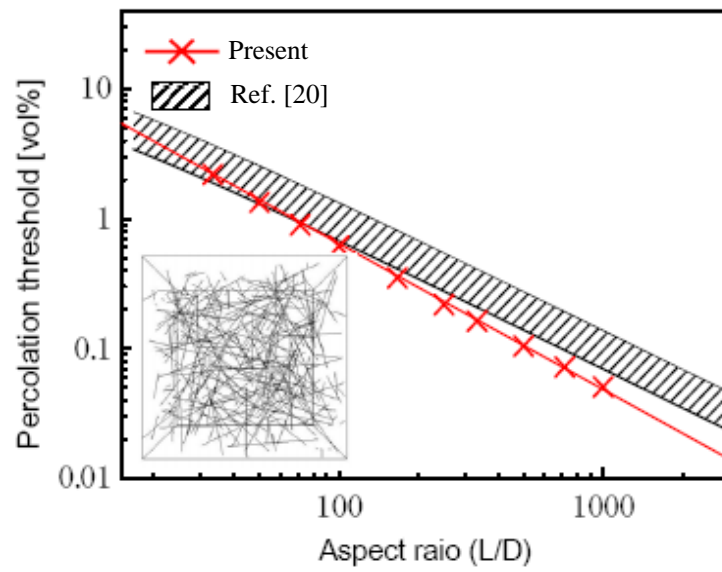


Figure 2.6. Percolation threshold versus aspect ratio of straight CNTs.

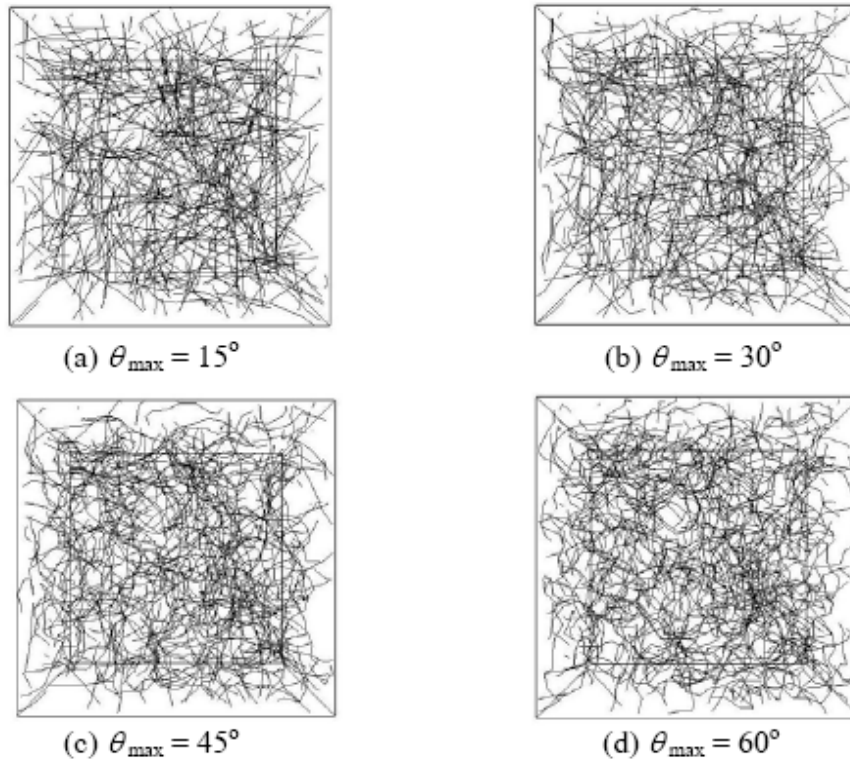


Figure 2.7. Schematic top view of models with curved CNTs for various θ_{\max} (top view).

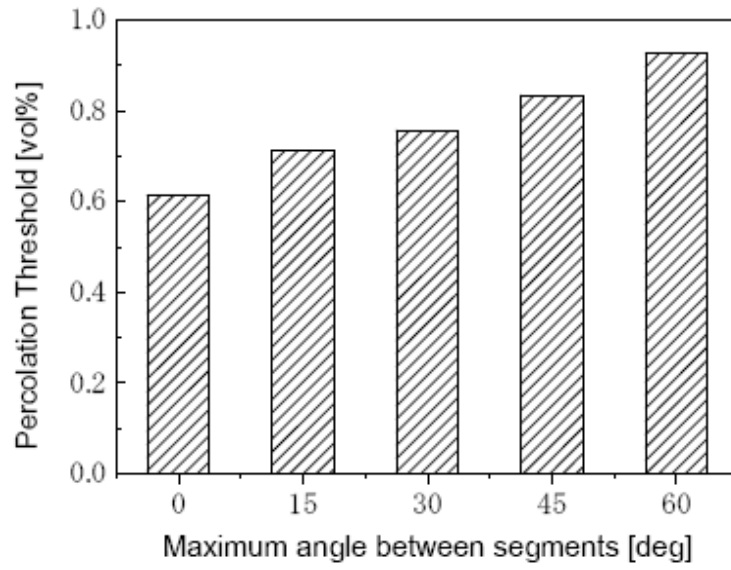


Figure 2.8. Influence of θ_{\max} on percolation threshold.

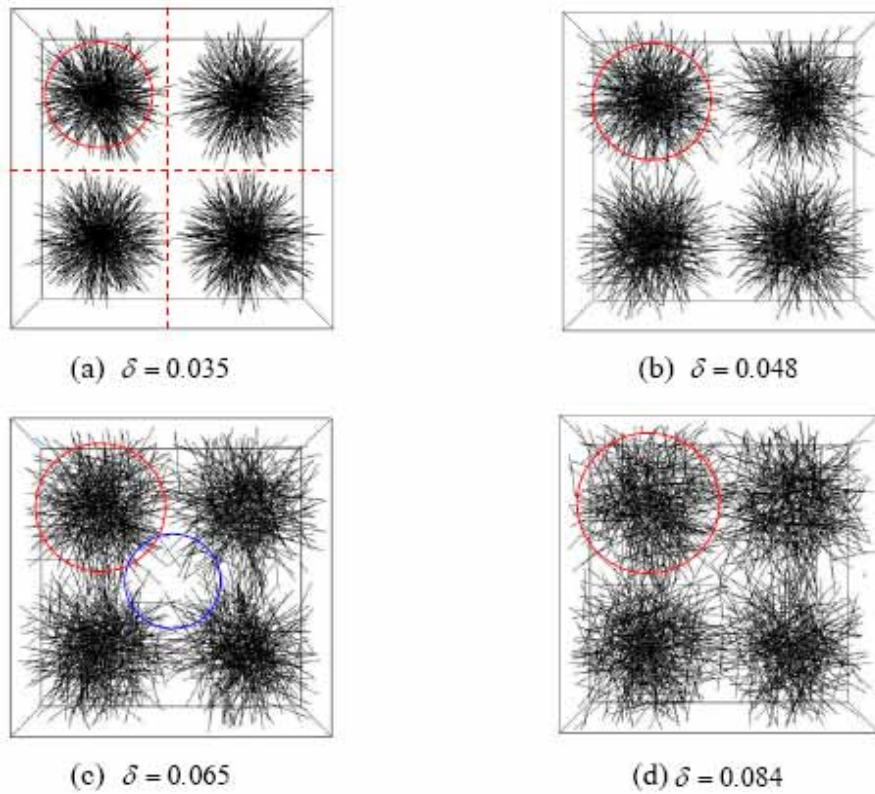


Figure 2.9. Schematic top view of agglomerated model generated by normal distribution (top view).

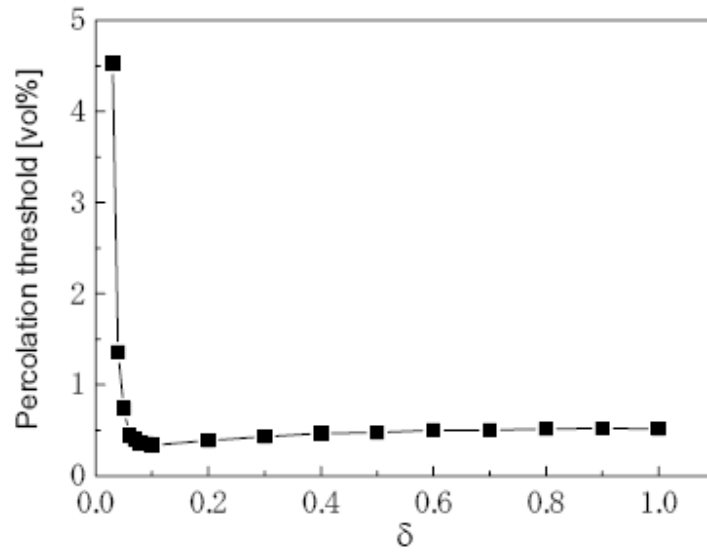


Figure 2.10. Influence of δ on percolation threshold.

3. PREDICTION OF ELECTRICAL CONDUCTIVITY OF NANOCOMPOSITES

In this section, we will proceed to the contents about the electrical conductivity of nanocomposites after the percolation threshold. First, we will introduce a 3D resistor network model for estimating the electrical conductivity of the 3D element with randomly distributed CNTs. Then, we will investigate the influences of various factors, such as the shapes of CNTs, aggregates of CNTs and the tunnel effect among CNTs on the electrical conductivity of nanocomposites.

3.1. A 3D Resistor Network Model for CNT/Polymer Nanocomposite

Traditionally, for the cases of a square lattice or a cubic lattice, if considering the sites occupied by fillers as conductors, and sites being not occupied by fillers as insulators, the electrical conductivity of composites can be evaluated by varying the volume fraction of filler from 0 to a value close to 1 [24, 25]. For the electrical conductivity after the percolation threshold, except the work in [22], there have been almost no numerical studies based on a fully 3D statistical network model, even for traditional electronic composites with filler materials such as short fibers or flakes.

In this research, we will try to construct a continuum system with randomly distributed CNTs. Unlike the studies [24, 25], in which the conductivity of a matrix phase is also modeled, in this research, the electrical paths in the matrix phase are completely neglected. Since the CNTs are randomly distributed in the matrix, for the matrix among CNTs, there are infinite paths if it is conductive. Here, to simplify our numerical model, the electrical conductivity of the matrix is taken as 0 S/m since the electrical conductivity of epoxy in this

study is around 10^{-12} S/m (resistivity is 10^{14} cm), which is much smaller than that of MWNTs.

As outlined above, we only consider the electrically-conductive paths or network formed by CNTs. A part of the network is shown in Figure 3.1(a). As shown in this figure, for two pre-existing CNTs i and $i+1$, a new CNT j is added into. Using the contact search algorithm stated previously, the contact state between CNT j and CNT i and CNT $i+1$ can be easily confirmed. The node numbers of two ends of CNT j are k and $k+1$, respectively. The intersections between CNT j and CNT i and CNT $i+1$ are numbered as $k+2$ and $k+3$, respectively. In this case, CNT j is divided into three segments. As shown in Figure 3.1(b), the conductance (inverse of resistance) of one segment between two adjacent nodes of the four nodes from k to $k+3$ is represented by $g_{k,k+2}$, $g_{k+2,k+3}$ and $g_{k+3,k+1}$, respectively.

For instance, the conductance between k and $k+2$, i.e., $g_{k,k+2}$ can be expressed as

$$g_{k,k+2} = \sigma_{CNT} \frac{S_{CNT}}{l_{k,k+2}} \quad (15)$$

where σ_{CNT} is the electrical conductivity of CNTs, $l_{k,k+2}$ the distance between the node k and the node $k+2$, and S_{CNT} is the cross-sectional area of CNTs.

Usually, it is very difficult to measure the electrical conductivity of a single CNT. For a SWNT, as reported previously, its electrical conductivity ranges from 17.2 S/m to 3.0×10^9 S/m [26-28]. For a MWNT, its electrical conductivity ranges from $5 \times 10^3 \sim 5 \times 10^6$ S/m [29, 30]. There is a lack of uniformity of electrical conductivity of SWNTs, which strongly depends on the atomic structural parameters, such as the chiral vector. In this research, we employ σ_{CNT} of MWNTs as 1×10^3 , 10^4 , 10^5 , 10^6 S/m, respectively.

Next, for the nanocomposite containing randomly distributed CNTs, as shown in Figure 3.2, the applied voltage is V , therefore, the electrical potentials of electrodes 1 and 2 are V and 0, respectively. Note that our model is a 3D one, for simplicity, only a 2D model is demonstrated. In our numerical computation, when the applied voltage is known, and the macroscopic current I of the nanocomposite can be calculated. As shown in Figure 3.2, at an arbitrary node i , the current is I_i , which is expressed as

$$I_i = \sum_{j, j \neq i}^N g_{ij} (V_i - V_j) \quad (16)$$

where N is the total number of nodes in the network, and g_{ij} is the conductance between the node i and the node j , V_i and V_j are the electrical potentials at the nodes i and j , respectively. Moreover, the following relationship $g_{ij} = g_{ji}$ holds. For those nodes, which are not directly connected to the node i by a CNT, we can set $g_{ij} = 0$ since the conductivity of matrix phase is taken to be zero.

By constructing Eq. (16) for all nodes, we can summarize the following linear algebraic equations as

$$\{I\} = [G]\{V\} \quad (17)$$

where $\{I\}$ is the vector of electrical currents, $\{V\}$ is the vector of electrical potentials, and $[G]$ of dimension of $N \times N$ is the conductance matrix, which is described as

$$G_{ij} = \sum_{j, j \neq i}^N g_{ij} \text{ and } G_{ij} = G_{ji} \quad (18)$$

When the nodes are not located on the two electrodes of the both sides of the nanocomposite in Figure 3.2, based on Kirchhoff's current law, there is

$$I_i = 0 \quad (19)$$

Also, for those nodes located on the two electrodes, their sum can be set up as

$$I = \sum I_i \quad (\text{Electrode1}) \quad (20a)$$

$$-I = \sum I_i \quad (\text{Electrode2}) \quad (20b)$$

For the components in the electrical potential vector corresponding to those nodes located on electrodes 1 and 2, they are set by

$$V_i = V \quad (\text{Electrode1}) \quad (21a)$$

$$V_i = 0 \quad (\text{Electrode2}) \quad (21b)$$

By substituting Eqs (19), (20) and (21) into Eq. (17), we can finally get the following equation

$$[A]\{x\} = \{B\} \quad (22)$$

Where the vector $\{x\}$ contains the unknown electrical currents and potentials, $[A]$ is still a symmetric matrix, and the vector $\{B\}$ contains the known electrical currents at the inner nodes, which are equal to zero as shown in Eq. (19), and potentials at the two electrodes as shown in Eqs (21).

The obtained I_i is substituted into Eq. (20) to get the total electrical current of electrodes, i.e., I . Since Eq. (22) is a large-scale linear algebraic equation, here we employ an iterative

solver, i.e., ICCG (Incomplete Cholesky Conjugate Gradient) to solve it. The obtained I as well as the applied known voltage V is then used in the following Ohm's law to get the macroscopic electrical conductivity of nanocomposite σ_{com} as follows

$$\sigma_{com} = \frac{I}{V} \frac{L_{com}}{S_{com}} \quad (23)$$

where S_{com} and L_{com} are the cross-sectional area and the length of the nanocomposite, respectively.

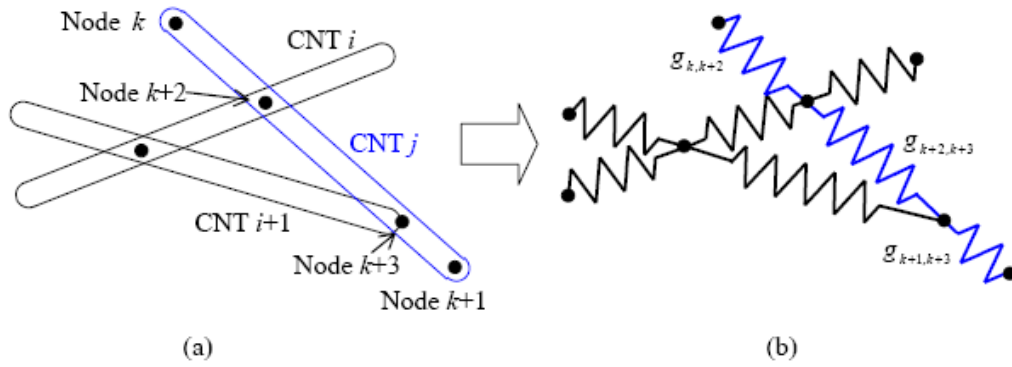


Figure 3.1. Modeling of electrical resistance in network formed by CNTs.

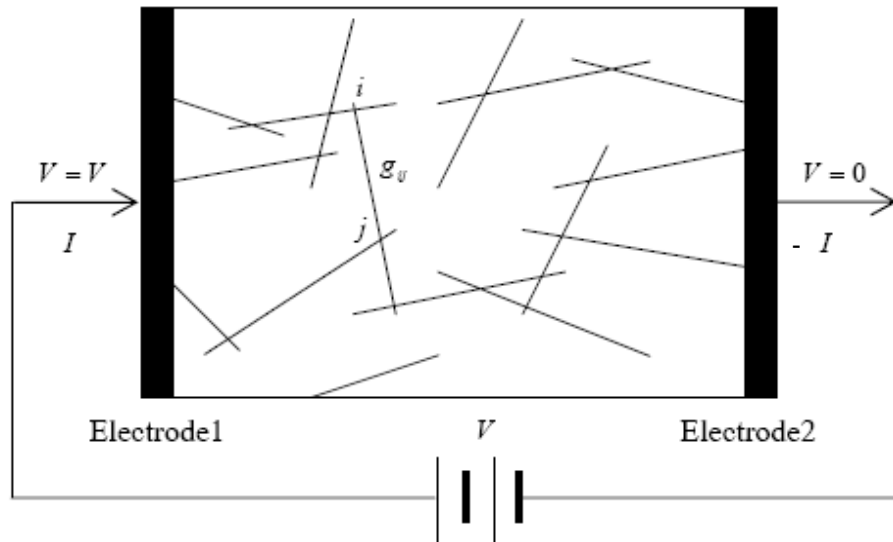


Figure 3.2. Random resistor network of CNTs.

3.2. Numerical Results of Model of Uniform Random Distribution of Straight CNTs in Matrix

First, for the case of uniformly and randomly distributed straight CNTs of $L/D=100$, the electrical conductivity of nanocomposites is shown in Figure 3.3(a) for various electrical conductivities of CNTs. This figure reveals that the electrical conductivity of nanocomposites increases as the electrical conductivity of CNTs increases.

If we consider the following traditional percolation theory for the electrical conductivity σ_{com} of composites [31] as follows

$$\sigma_{com} = \sigma_0 (\phi - \phi_c)^t \text{ for } \phi > \phi_c \quad (24)$$

where t is the critical exponent, ϕ the volume fraction of filler, ϕ_c the percolation threshold, and σ_0 is a parameter. Usually ϕ_c and σ_0 are determined experimentally.

By using the electrical conductivities at two volume fractions of CNTs obtained from numerical simulations, we can identify the critical exponent t as follows

$$t = \frac{\log(\sigma_{com1}/\sigma_{com2})}{\log\{(\phi_1 - \phi_c)/(\phi_2 - \phi_c)\}} \quad (25)$$

Here, for an ideal state of uniform random distribution of straight CNTs in a polymer, by using Eq. (25) and the least-squares fitting, from the numerical results for various σ_{CNT} (10^3 S/m~ 10^5 S/m), we have identified that the average value of t is 1.8 ± 0.05 (see Figure 3.3(b)), which is universal and depends on the dimensionality of the system [32]. In a 3D system, the expected value is 2.

Figure 3.4 shows the results of electrical conductivity with respect to the different aspect ratios of CNTs (L/D) when $\sigma_{CNT}=10^4$ S/m. For the case of $L/D=100$, the computation can be carried out up to around 6.0% volume fraction of CNTs. However, for the case of $L/D=1000$, the computation can only be performed up to 0.5% volume fraction of CNTs. The reason is that as L/D increases, the diameter and volume of CNTs should be decreased since the length of CNTs is fixed in our numerical models as stated in Section 2.2.1. For the high volume fractions of CNTs of high aspect ratios, the number of CNTs increases remarkably, which results in a large-scale amount of computation. This tremendous computational amount is already over than capacity limit of a personal computer. Also, in Figure 3.4, it can be identified that the percolation threshold tends to decrease as L/D increases. When the electrical conductivity of nanocomposites attains at 10 S/m (red line in Figure 3.4(a)), the corresponding volume fraction of CNTs for $L/D=100$ is around 1.3 vol%, meanwhile, the volume fraction of CNTs for $L/D=1000$ is only around 0.3 vol%. It means that for the applications, such as electromagnetic interference materials, it is better to use CNTs with the high aspect ratio under the condition of uniform dispersions. Of course, it is well-known that practically it is more difficult to disperse the longer CNTs uniformly in matrix. The fitted critical exponent t in this figure is still equal to 1.8 as shown in Figure 3.4(b), which means that the aspect ratio of CNTs does not influence the value of critical exponent.

3.3. INFLUENCE OF SHAPES AND AGGREGATES OF CNTs ON ELECTRICAL CONDUCTIVITY OF NANOCOMPOSITES

Next, the influence of the curved shape of CNTs is investigated, which is shown in Figure 3.5(a) for the case of $\sigma_{CNT}=10^4$ S/m and $L/D=100$. The number of divisions of straight CNTs is 10. From this figure, it can be found that the electrical conductivity of nanocomposites decreases as θ_{max} increases. Furthermore, from Figure 3.5(b), we can find that when $\phi - \phi_c$ ranges from 0.003 to 0.01, the slope of the results of curved CNTs is almost same as that of straight CNTs, i.e., $t=1.8$. However, when $\phi - \phi_c$ is larger than 0.01, the slope of the results of curved CNTs tends to be slightly lower, i.e., $t=1.6$. It means that over a limit of the volume fraction of CNTs, the formation of network by the curved CNTs is more difficult than that by the straight CNTs.

We further explore the influence of aggregates of CNTs in matrix for the case of $\sigma_{CNT}=10^4$ S/m and $L/D=100$, which is shown in Figure 3.6(a). Here, δ is a parameter to represent the extensity of aggregates in Eq. (14). As δ decreases, the electrical conductivity of nanocomposites becomes lower. Also, for the cases of $\delta = 0.065$ and $\delta = 0.056$, the continuous electrical conductivity with respect to the volume fraction of CNTs can be obtained, whereas, when $\delta \leq 0.048$, there are strong discontinuities in the results. When $\delta=0.035$, the electrical conductivity of nanocomposites almost remains to be constant. The reason can be found from Figure 2.9. When $\delta=0.065$ as shown in Figure 2.9(c), there are a lot of CNTs located between the isolated aggregates, which connect aggregates together and form the network easily. However, when $\delta=0.035$, as shown in Figure 2.9(a), there are very few CNTs located between isolated aggregates, which leads to the difficult formation of conductive network, and the low and constant electrical conductivity of nanocomposites. Even with the addition of new CNTs, due to the limit from the formation of aggregate model with centered normal distribution, it is hard for these newly added CNTs to play a bridge between two aggregates. For the discontinuities in the results of $\delta=0.042$, which happens at 2.5 vol% and 3.5 vol%, the reason may also be from that the addition of only a few CNTs, which however connect isolated aggregates together, can result in a sudden increase of electrical conductivity of nanocomposites. From the above results, we can find that the influence of aggregates is more significant than that of the curved shape of CNTs. Moreover, in Figure 3.6(b), the influence of aggregates is obvious, which leads to the much lower t .

3.4. Influence of Tunnel Effect Among CNTs on Electrical Conductivity of Nanocomposites

Usually, in the stage just before the percolation threshold, although a complete electrically-conductive path has not been formed, there may be a very weak electrical conductivity due to the short distances among CNTs as shown in Figure 1.1(b). These short distances among CNTs can result in the possible tunnel effect to transfer electric charges among CNTs. A lot of the situations of CNTs of short distances have been identified through our SEM observations as shown in Figure 3.7.

For this tunnel effect, as shown in Figure 3.8, we can approximately evaluate the resistance between two separated CNTs with a short distance as [33]:

$$R_{tunnel} = \frac{V}{AJ} = \frac{h^2 d}{Ae^2 \sqrt{2m\lambda}} \exp\left(\frac{4\pi d}{h} \sqrt{2m\lambda}\right) \quad (26)$$

where J is tunnel current density, V the electrical potential difference, e the quantum of electricity, m the mass of electron, h the Planck's constant, d the barrier width (i.e., the distance between CNTs), λ the height of barrier (for epoxy, 0.5 eV~2.5 eV), and A the cross-sectional area of tunnel (we simply use that of CNTs here).

The influence of tunnel effect is shown in Figure 3.9. From it, we can find that the tunnel effect leads to the increase of electrical conductivity, but its effect is limited to a very narrow band around the percolation threshold. This finding highlights that the application of this nanocomposite for highly sensitive strain sensor should be focused on the region around the percolation threshold, which was also experimentally verified by other researchers, e.g. [34].

3.5. An Empirical Percolation Theoretical Model

To obtain a simple percolation theory from the numerical results with the assumption of the uniform random distribution of straight CNTs in the polymer, we need to identify some important terms. For the critical exponent t , as shown above, it is a constant, i.e., 1.8, which does not depend on the aspect ratio of CNTs. Also, for the percolation threshold ϕ_c , as shown in Eq. (13) in Section 2.1, it relates to the aspect ratio in a very simple form. Now, we still need to find σ_0 in Eq. (24). Usually, from the explanation of traditional percolation theory, σ_0 is the conductivity of the element of a percolating network [31], i.e., the conductivity of CNTs here.

Here, we explore σ_0 again from Figure 3.4. If we use the identified t and ϕ_c into Eq. (24), we can obtain the following equation

$$\sigma_{com} = \sigma_0 \left\{ \phi - \left(\frac{L}{D} \right)^{-1.1 \pm 0.03} \right\}^{1.8 \pm 0.05} \quad (27)$$

where ϕ is the volume fraction of CNTs.

By fitting the results of various aspect ratios to determine σ_0 , the results of σ_0 normalized by σ_{CNT} are shown in Figure 3.10. From this figure, we have surprisingly found that σ_0 is a parameter, which not only depends on σ_{CNT} , but also on the aspect ratio of CNTs as follows

$$\frac{\sigma_0}{\sigma_{CNT}} = 10^{0.85\{\log(L/D)-1\}} \quad (28)$$

Finally, the percolation theory in Eq. (24) can be re-cast into the following simple form,

$$\sigma_{com} = \sigma_{CNT} \cdot 10^{0.85\{\log(L/D)-1\}} \cdot \left\{ \phi - \left(\frac{L}{D} \right)^{-1.1 \pm 0.03} \right\}^{1.8 \pm 0.05} \text{ for } \phi > \phi_c \quad (29)$$

We note that the percolation threshold expression, i.e., $(L/D)^{-1.1}$ is only valid for filler particles of high L/D , such as over 10. This model is of great significance by which the macroscopic electrical conductivity of nanocomposites can be predicted simply if we know σ_{CNT} and L/D of CNTs. The theoretically predicted results by Eq. (29) are compared with those obtained numerically as shown in Figures 3.11(a) and 3.11(b) for various aspect ratios of CNTs and various electrical conductivities of CNTs. As shown in Figure 3.11, both results agree with each other very well. This model is also useful for predicting the electrical properties of traditional electronic composites using short fibers of high L/D (e.g., higher than 10) as filler particles.

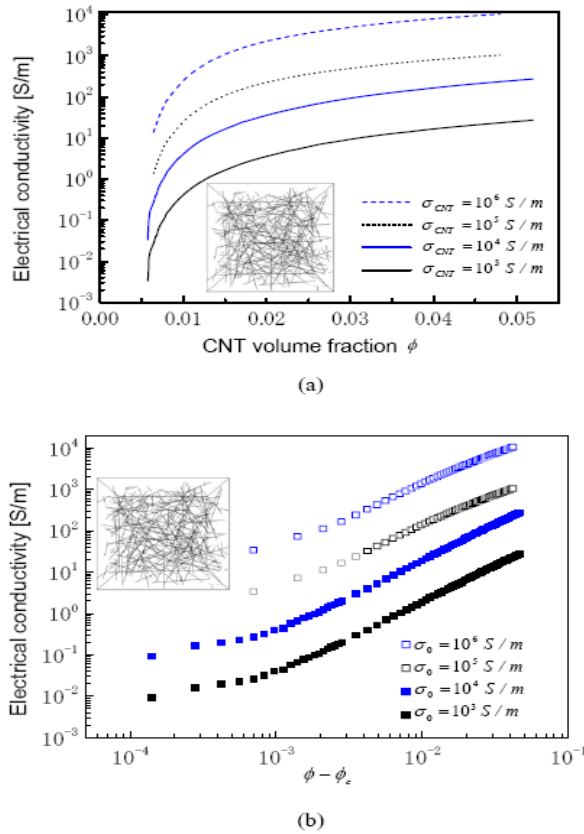
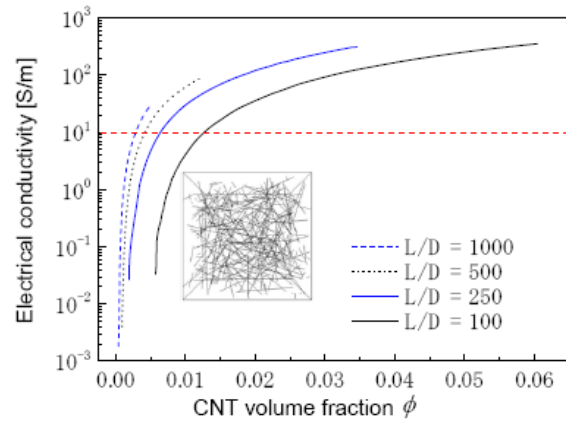
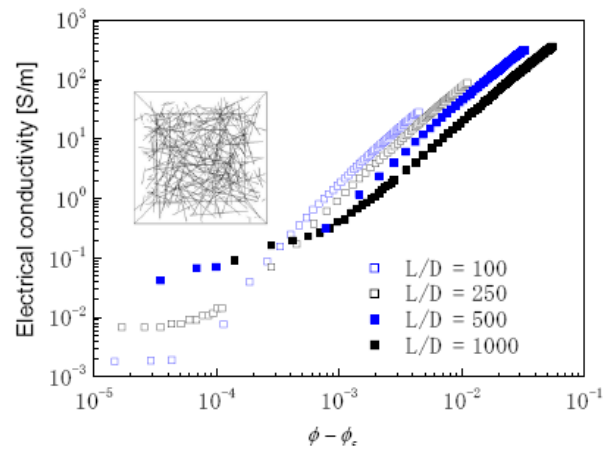


Figure 3.3. Electrical conductivity of nanocomposite for various conductivities of CNTs: (a) Electrical conductivity versus volume fraction of CNTs; (b) Electrical conductivity versus reduced volume fraction of CNTs.



(a)



(b)

Figure 3.4. Electrical conductivity of nanocomposite for various aspect ratios of CNTs: (a) Electrical conductivity versus volume fraction of CNTs; (b) Electrical conductivity versus reduced volume fraction of CNTs.

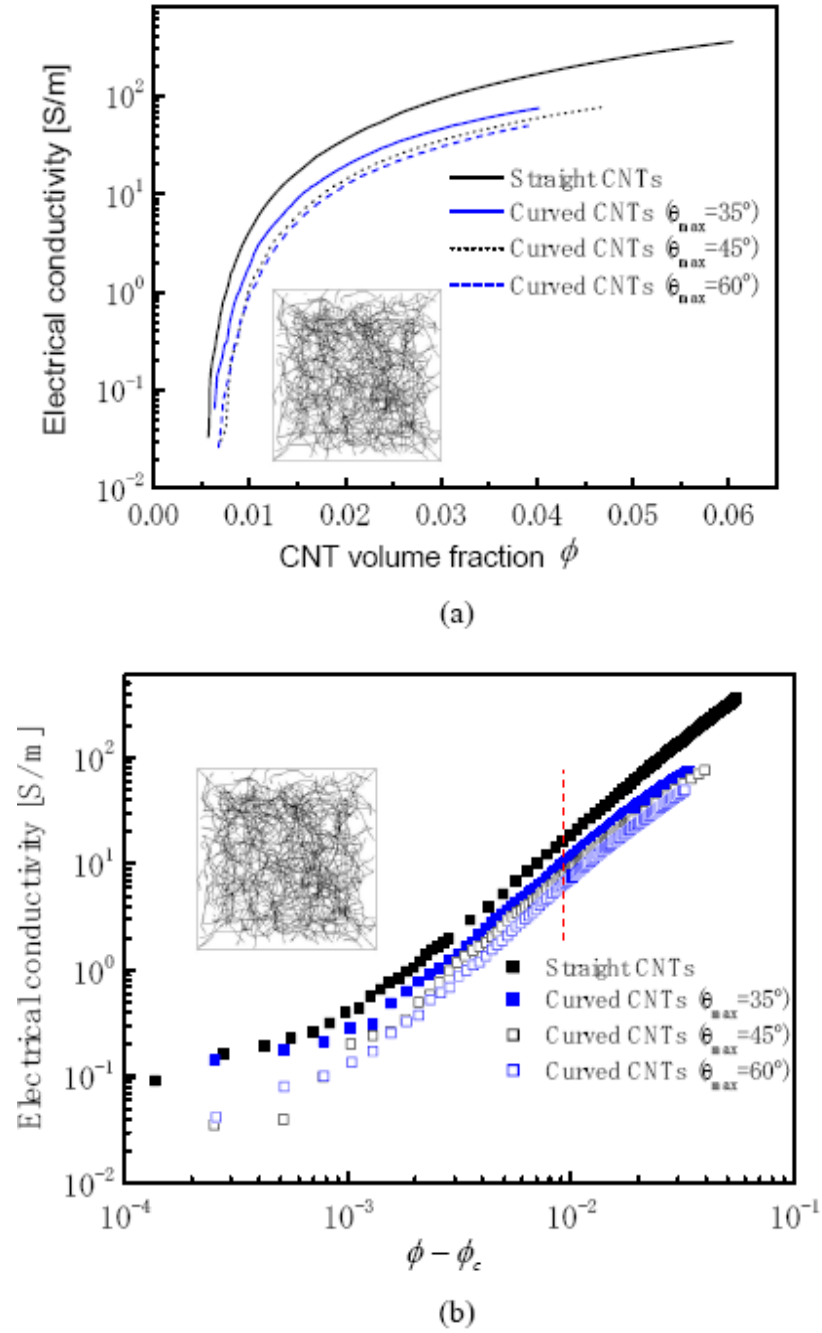


Figure 3.5. Electrical conductivity of nanocomposite for various θ_{max} of CNTs: (a) Electrical conductivity versus volume fraction of CNTs; (b) Electrical conductivity versus reduced volume fraction of CNTs.

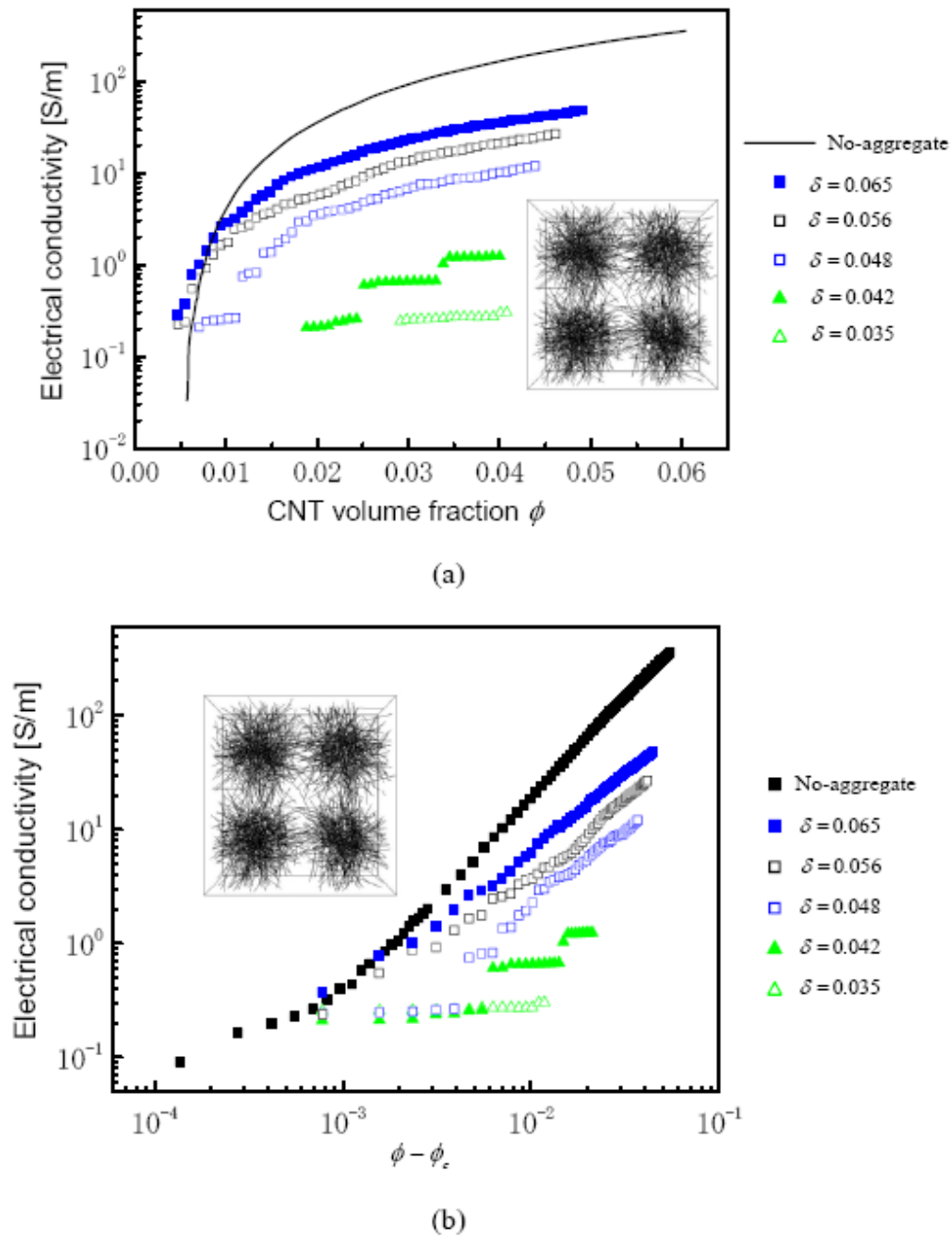


Figure 3.6. Electrical conductivity of nanocomposite for various aggregation model: (a) Electrical conductivity versus volume fraction of CNTs; (b) Electrical conductivity versus reduced volume fraction of CNTs.

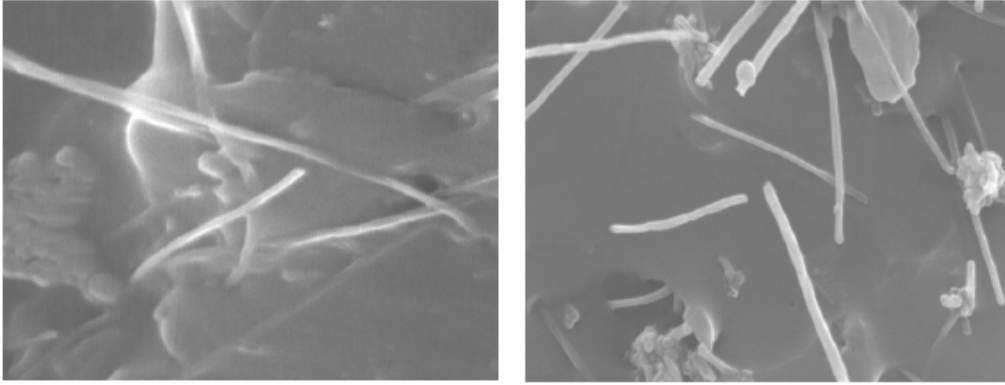


Figure 3.7. Configurations of some close CNTs in nanocomposite.

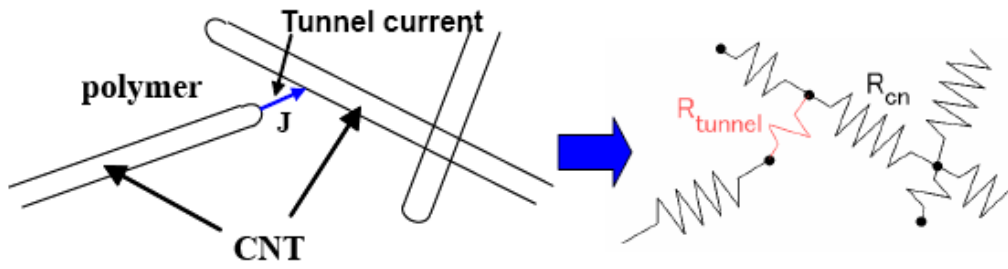


Figure 3.8. Modeling of tunnel effect among CNTs.

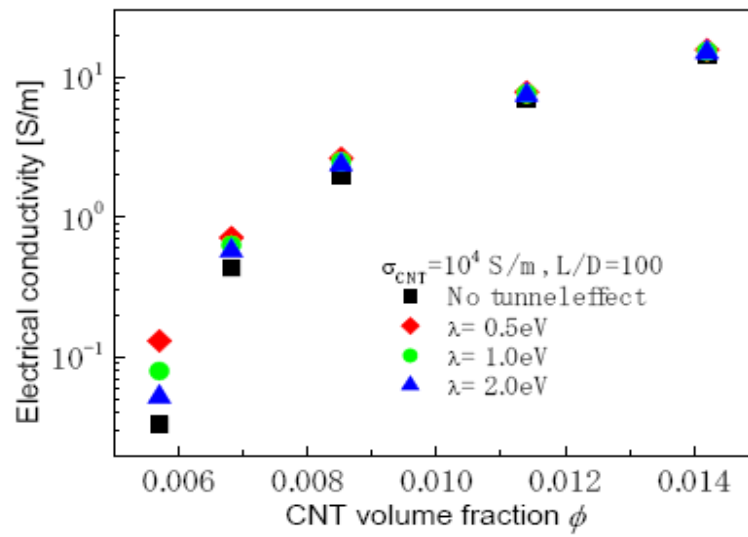


Figure 3.9. Influence of tunnel effect on electrical conductivity of nanocomposite.

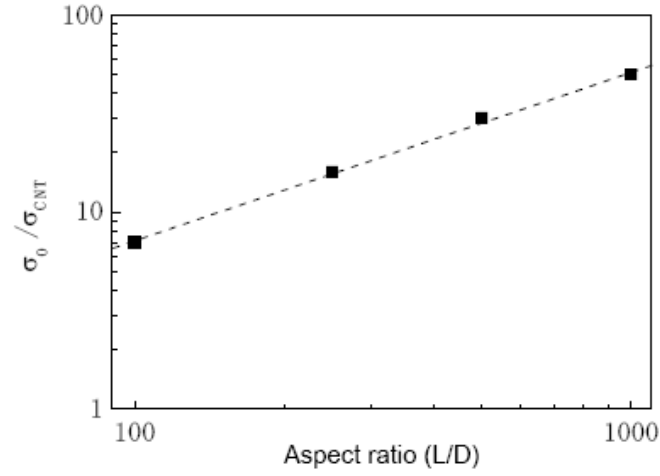
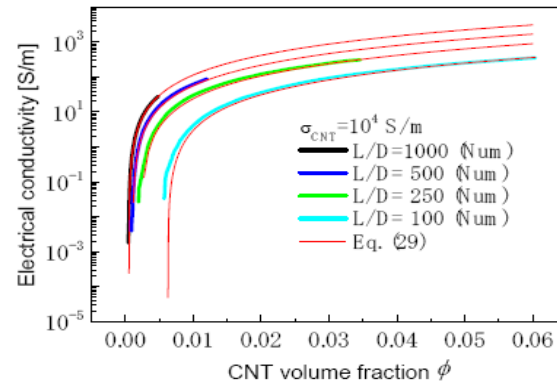
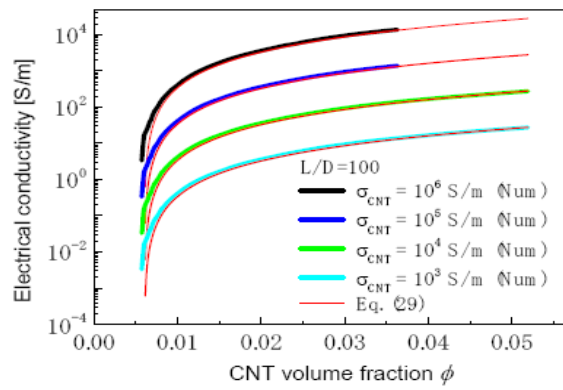


Figure 3.10. Relation between σ_0 / σ_{CNT} and aspect ratio of CNTs.



(a)



(b)

Figure 3.11. Verification of proposed percolation theory by numerical results: (a) Comparison of theoretical results of Eq. (29) and numerical results for various aspect ratios of CNTs; (b) Comparison of theoretical results of Eq. (29) and numerical results for various electrical conductivities of CNTs

4. EXPERIMENTS

In this section, we will report our experimental results for the electrical properties of this nanocomposite, which was fabricated using in situ polymerization method.

4.1. Fabrication Process of Nanocomposites

A kind of MWNTs made from chemical vapor deposition (CVD), which was provided by Nano Carbon Technologies Co. (NCTC) in Japan, was used. The reasons to choose MWNT as filler are from that they are generally conducting and their dispersion is comparatively easier due to their much lower absorption energy compared with that of SWNTs (around one order of magnitude lower). Furthermore, the price of MWNTs is much cheaper than that of SWNTs. The purity of these MWNTs is higher than 99.5%. The diameter of MWNTs ranges from 20 nm to 80 nm, and the average length of MWNTs is around 5 μm , respectively. The average aspect ratio of MWNTs is around 100. The reported electrical conductivity of MWNTs ranges from 5×10^3 S/m to 5×10^6 S/m [20, 21]. A kind of insulating epoxy (bisphenol-F resin) was employed here. The electrical conductivity of epoxy is around 10^{-12} S/m. The reason for using bisphenol-F resin instead of bisphenol-A resin [10, 11] is that its viscosity is lower. An amine hardener (polyaminoamides) was used in our experiments, which cures epoxy resins by reacting with the epoxide groups or by promoting self-polymerization of the epoxy by catalytic action. The epoxy and hardener are in the liquid state at room temperature. A planetary mixer with two rotation axes is shown in Figure 4.1. A cup containing the mixture of epoxy and CNTs is in an orbital motion around the X_1 axis. Also, the cup rotates around its central axis, i.e., the X_2 axis, which is vertical to the top and bottom planes of cup. Usually, the rotation speed ω_2 around the X_2 axis is comparatively very slow, which is 2.5 times lower than ω_1 around the X_1 axis. The highest rotation speed of ω_1 is 2000 rpm. In the mixing process, the shear forces provided by the planetary mixer can be much higher than that of a conventional propeller stirrer. Originally, in our preparing process of nanocomposites, we pre-treated the CNTs in a solvent using a sonication bath. However, it was found that the effect of this step on the final electrical performance of nanocomposites is not so obvious. Therefore, MWNTs without further treatment were employed directly. For the fixed amount of MWNTs loading, i.e., 2.0 wt%, 5 samples were prepared using the different parameters in the fabrication process, which are described as follows:

Sample A: The epoxy and hardener were first poured into the cup. They were mixed using the mixer for 20 seconds with ω_1 at 2000 rpm. Then, CNTs were added into the mixture, which was mixed again for 1 minute with ω_1 at 800 rpm.

Sample B: The epoxy and hardener were first poured into the cup. They were mixed using the mixer for 20 seconds with ω_1 at 2000 rpm. Then, CNTs were added into the mixture, which was mixed again for 1 minute with ω_1 at 2000 rpm.

Sample C: The epoxy was poured into the cup, and then CNTs were added into the epoxy. They were mixed using the mixer for 1 minute with ω_1 at 2000 rpm. Then, the hardener was poured into, and the mixture was mixed again for 1 minute with ω_1 at 2000 rpm.

Sample D: The epoxy was poured into the cup, and then CNTs were added into the epoxy. They were mixed using the mixer for 4 minutes with ω_1 at 2000 rpm. Then, the hardener was poured into, and the mixture was mixed again for 1 minute with ω_1 at 2000 rpm.

For all above samples, after the mixing process, the liquid was cast in a silicon mold to form the nanocomposites, which was cured in a vacuum oven at 80°C for 3 hours to remove excess air.

Sample E: The steps are the same as those in Sample D, except the different curing process, where the final mixture was cured at room temperature for 48 hours.

After the curing and deforming process, the surfaces of two sides of specimens were covered with silver paste to ensure good contact of the sample surfaces with the electrodes as shown in Figure 4.2. Copper wire was used as electrode material. The conductivity was measured in dry air at ambient temperature by a four-terminal method using a LCR meter (HIOKI 3522-50) as shown in Figure 4.2. The applied voltage ranged from 0.01 V to 5 V to investigate the dependence of DC electrical properties on the applied voltage. For each sample, five specimens were prepared for obtaining the average electrical properties of nanocomposites. To check the uniformity of resistance distribution, 4 vertical wires are inserted into the specimen of Sample D along the length direction as shown in Figure 4.3. As shown in Figure 4.4, the resistance distribution along the length direction is almost constant. The isotropy of electrical resistance of specimen of Sample D along length, width and thickness directions was also checked.

4.2. Effect of Parameters in Fabrication Process on Electrical Properties of Nanocomposites

The effects of curing process on the electrical conductivity of nanocomposite are shown in Figure 4.5. Note that the resistance of Sample E is too large, which exceeds the measurement limit of the LCR meter of 200 M Ω used. It means that the electrical conductivity of Sample E is lower than a value at the order of 10^{-6} S/m if we consider the dimensions of specimen. This result is not shown in this figure. The obtained electrical conductivity of various specimens ranges from the order of 10^{-6} S/m to the order of 1.0 S/m depending on the different fabrication processes used.

By comparing the result of Sample D shown in Figure 4.5 and the result of Sample E (lower than 10^{-6} S/m), we can find that the result of Sample E cured at room temperature for 48 hours is much lower than that of Sample D cured in the vacuum oven at 80°C for 3 hours. This finding is coincident with that in [12], where it was shown that high curing temperature enhances the conducting network formation of nanotube clusters by enhancing mobility of CNTs in the accelerated diffusion process.

Next, we investigate the influence of mixing time of the mixture of epoxy containing MWNTs. From the results of Samples C and D, we can find that the result of Sample D with a longer mixing time (4 minute) is 3 times lower than that of Sample C (1 minute). It means that too long mixing time is not beneficial for enhancing the electrical properties of nanocomposites. Generally, it may be helpful to keep the state of small-scale or mild aggregates of MWNTs in the dispersion process, which make the formation of macroscopic conducting network more easily in the reaggregation process of MWNTs after adding

hardener [12]. Therefore, this phenomenon may be explained from that a too long mixing process may break up the small aggregates by overcoming the effect of Van der Waals forces among CNTs, which has a negative impact on the formation of network.

For the mixing speed, from Figure 4.5, we can find that the result of Sample A is around 10 times higher than that of Sample B although the mixing speed of Sample A is much lower than that of Sample B. The reason is that with the addition of hardener, small nanotube aggregates are formed, which subsequently agglomerate to form a macroscopic network covering large volume fractions of the epoxy as shown in Figure 4.6(a). In this case, low shear forces, which provide the particles with sufficient kinetic energy to overcome the repulsive interactions of the electrostatic charging, are helpful to induce the agglomeration [12]. However, using higher shear forces in this step can disrupt the agglomerates as shown in Figure 4.6(b). Similarly to that shown previously for the effect of longer mixing time, the effect of higher mixing speed on the electrical performance of nanocomposites can be negative.

We further explore the influence of the timing for adding the hardener. Note that all of previous studies employed the similar procedure of Samples C and D, in which the hardener was added after the dispersion process of MWNTs in epoxy. By comparing the results of Samples C and B, we can interestingly find that the result of Sample B is around 3 times higher than that of Sample C. Therefore, like the process used in Sample B, it is at least harmless to mix the epoxy and hardener first with the subsequent addition of MWNTs. It is very difficult to clearly explain this phenomenon. One reason may be from the easier formation of macroscopic network in the polymerization process accompanied by the dispersion process of MWNTs. But another reason may be that the procedure of Sample B can partially avoid the encapsulation or coating phenomenon of CNTs. Although the exact mechanism of how MWNTs interact with polymer is still unclear, the practical encapsulation of nanotubes by polymer chains has been identified in many previous studies [9, 19], which retards the conducting between CNTs. Therefore, avoidance of possible encapsulation of nanotubes by polymer chains is a very important issue.

Some fractured cross sections for Samples A, B, C and D were observed using a SEM (HITACH S-4300E) as shown in Figures 4.7 and 4.8. From these figures, it can be found that there is no obvious difference on the fractured surfaces in various samples by different processes although the electrical conductivities of these samples are much different, e.g., the result of Sample D is around 100 times lower than that of Sample A. In these figures, as observed in [19], the comparatively homogeneous dispersion of CNT in polymer without very heavily concentrated aggregates can be identified clearly. Therefore, unlike SWNTs [6], heavily concentrated aggregates or bundling between MWNTs in matrix due to attractive Van der Waals forces do not exist if a proper mixing process is employed.

Finally, the above investigations indicate that the high curing temperature accelerates the formation of agglomeration, which is beneficial for enhancing the electrical properties of nanocomposites. However, an excessive long and powerful mixing process has a negative impact on the electrical performance of nanocomposites due to the difficult formation of macroscopic conducting network. Naturally, a mixing process with shear forces of a certain level is still necessary to stably disperse MWNTs in matrix by overcoming the heavily concentrated bundling of CNTs caused by high attractive Van der Waals forces, and to induce agglomeration by overcoming the repulsive forces among CNTs contributed by the electrostatic effect after addition of the hardener.

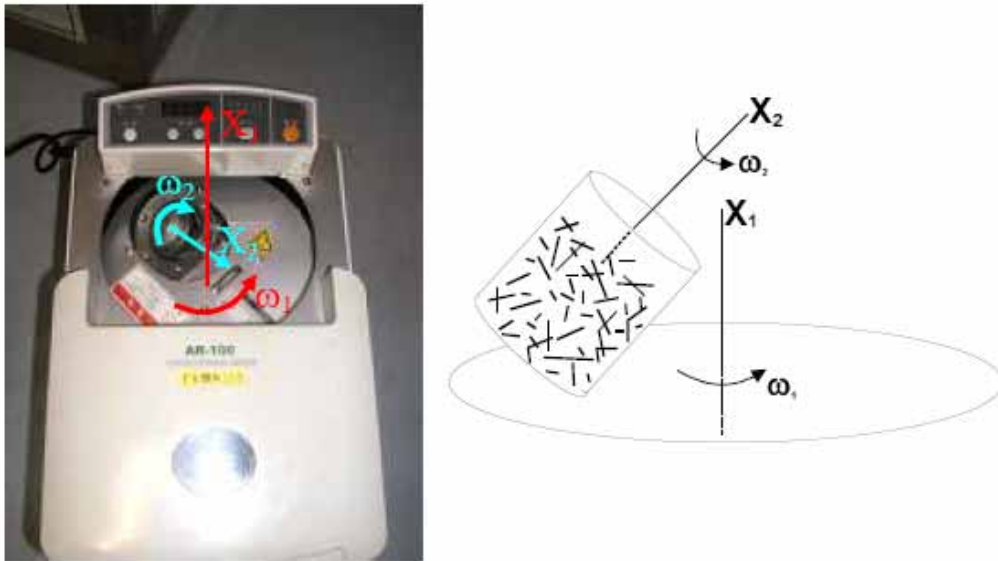


Figure 4.1. Description of a planetary mixer with two rotation axes.

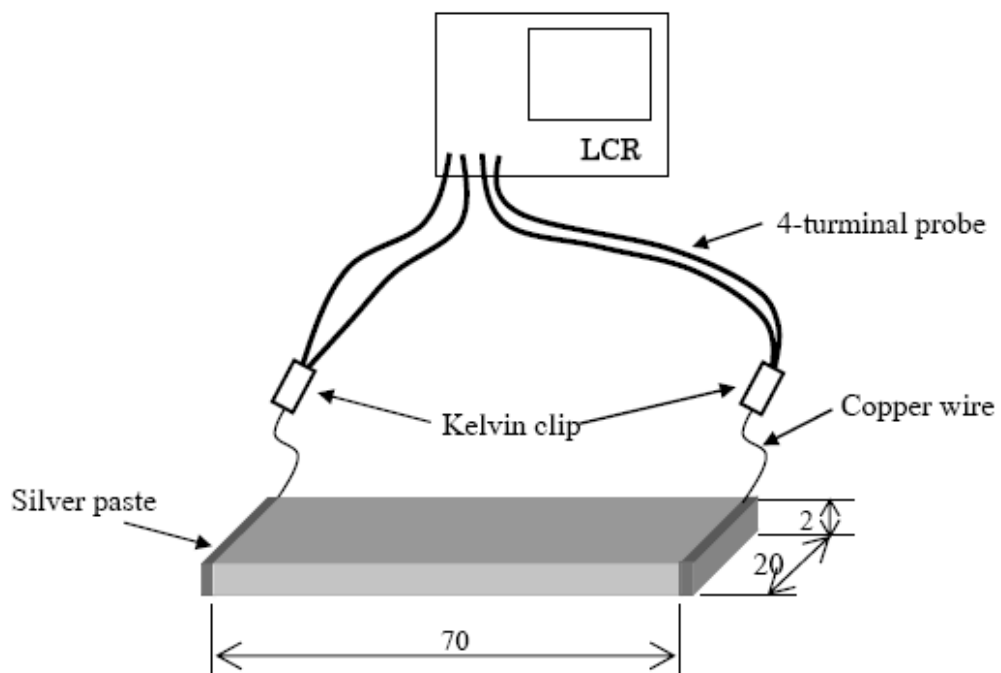


Figure 4.2. Schematic view of measurement of nanocomposite resistance (unit of length: mm).

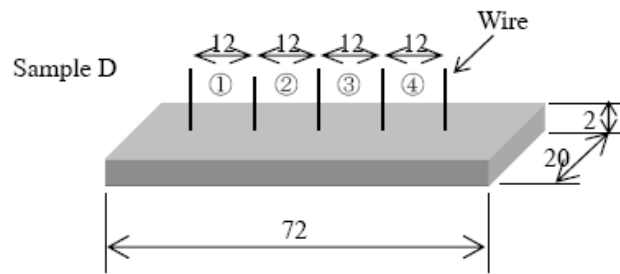


Figure 4.3. Specimen for checking resistance distribution (unit of length: mm).

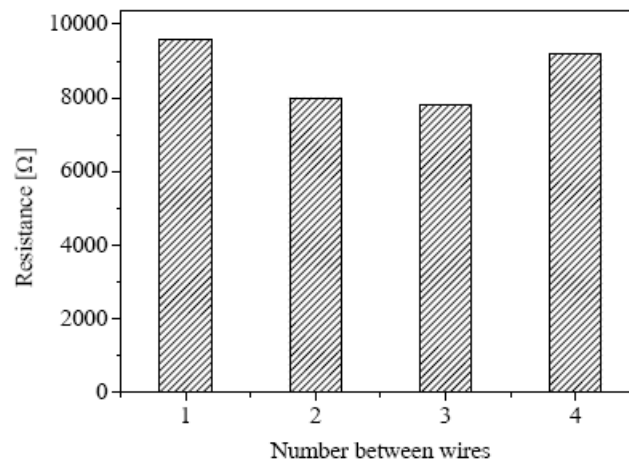


Figure 4.4. Resistance distribution between two adjacent wires.

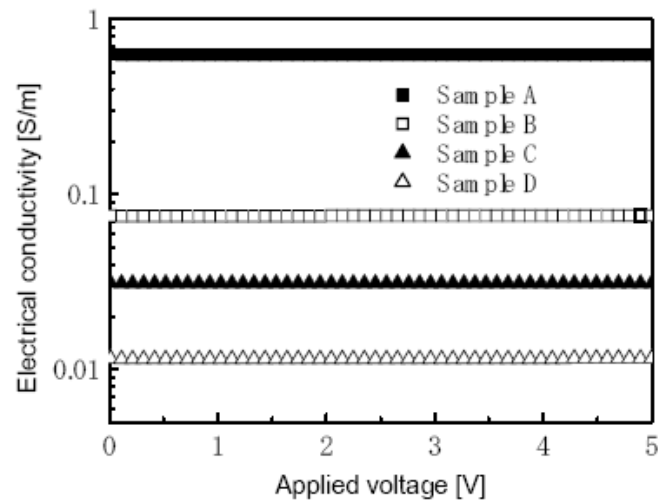
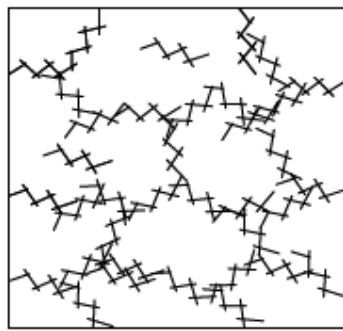
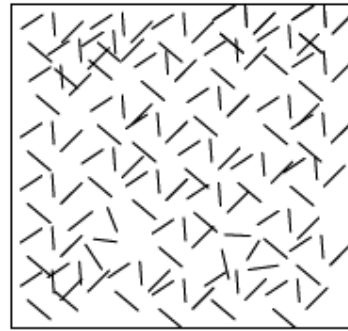


Figure 4.5. Electrical conductivities of various samples.



a) Conducting macroscopic network



b) Non-conducting macroscopic network

Figure 4.6. Comparison of two kinds of macroscopic networks.

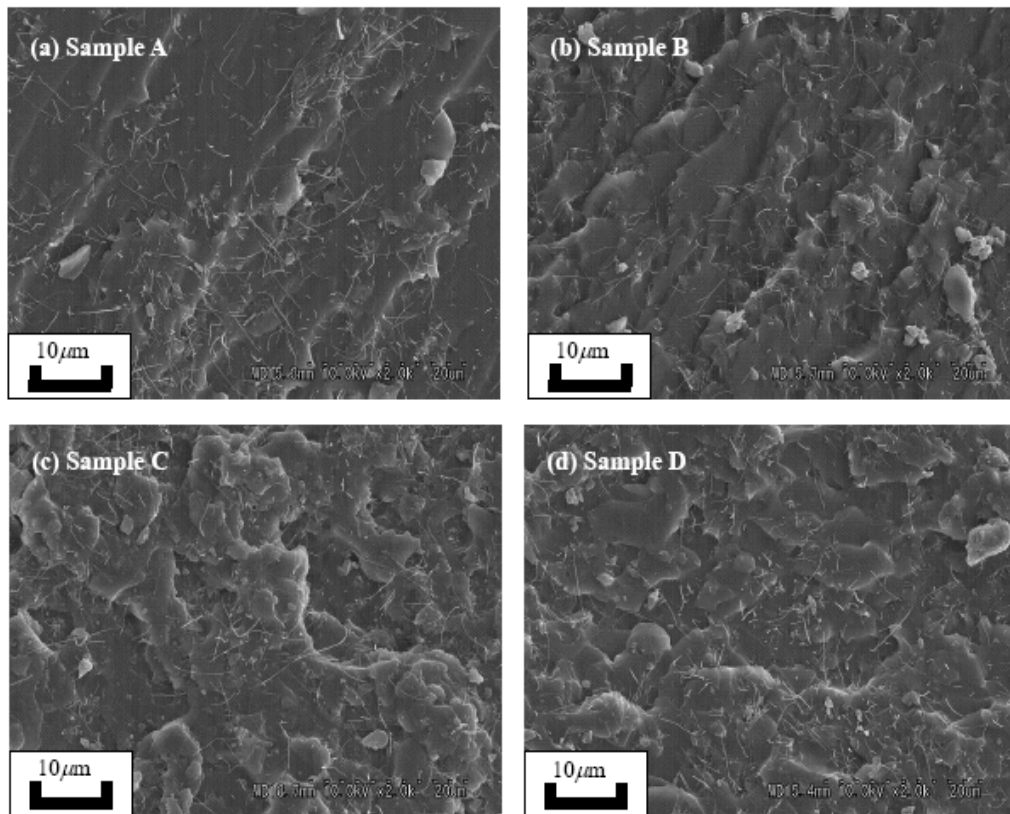


Figure 4.7. SEM images of nanocomposites for Samples A, B, C and D (2000 times magnification).

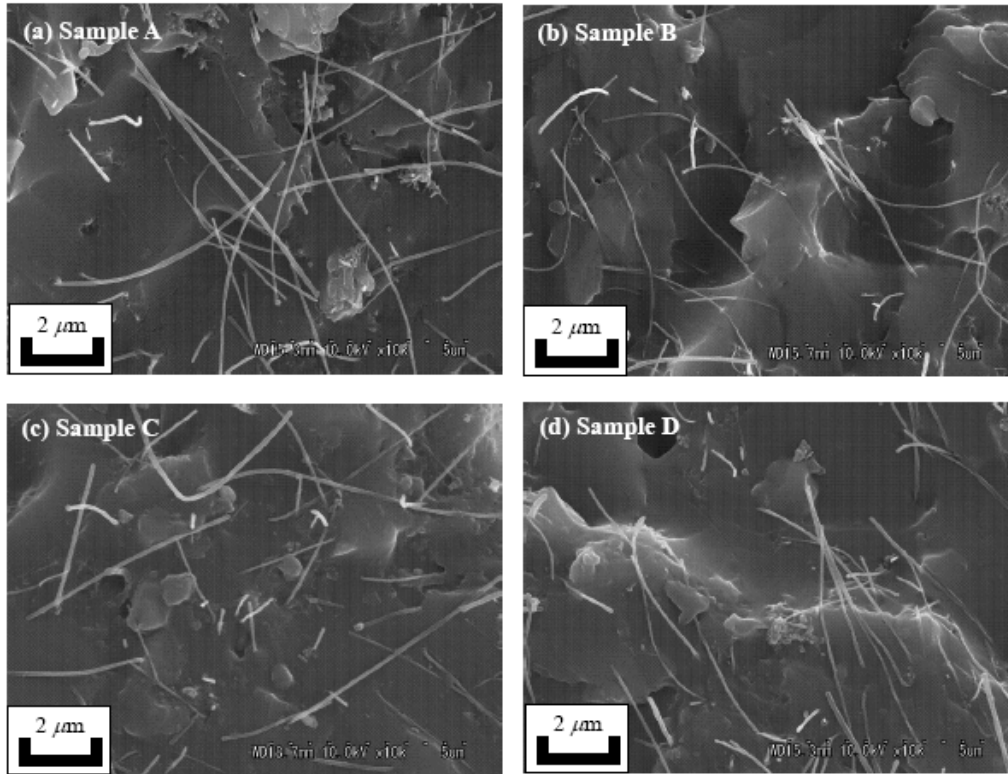


Figure 4.8. SEM images of nanocomposites for Samples A, B, C and D (10000 times magnification).

5. COMPARISON BETWEEN NUMERICAL AND EXPERIMENTAL RESULTS

To investigate the electrical conductivity versus MWNTs loading, finally, we prepared the specimens using the process of Sample B consistently. Specimens corresponding to 0.1, 0.3, 0.5, 1.0, 1.5, 2.0, 2.5, 3.0, 3.5, 4.0, 5.0, 6.0, 8.0, 10.5, 13.0 and 15.0 wt% of MWNTs loading, respectively were prepared. Although the electrical conductivity of Sample A is much higher than that of Sample B (around 10 times higher), the reason for not using the process of Sample A is that for higher volume fractions of MWNTs, the viscosity of the mixture containing MWNTs is very high. Therefore, it is hard to mix it using only 800 rpm as that in the procedure of Sample A for only 2.0wt%.

The present numerical and various experimental percolation thresholds versus the aspect ratio of CNTs are compared in Figure 5.1 in the volume fraction of MWNTs. The result of an empirical excluded volume approach [20] was also plotted. In our experiments, at first, the weight fraction of MWNTs was measured easily, and then the conversion between the volume fraction of MWNTs and the weight fraction of MWNTs was carried out as follows

$$\phi_{vol} = \frac{1}{1 + \frac{\rho_{CNT}}{\rho_{Poly}} \left(\frac{1}{\phi_{wt}} - 1 \right)} \quad (30)$$

where ϕ_{vol} is the volume fraction of MWNTs, and ϕ_{wt} is the weight fraction of MWNTs, and the mass density ρ_{CNT} of MWNTs and ρ_{Poly} of epoxy are 2100 kg/m³, and 1100 kg/m³, respectively.

Our experimental percolation threshold is 0.055 vol% (i.e., 0.1 wt%), which is quite low although it is not the lowest one as shown in Figure 5.1. If the procedure for Sample A was employed, a further lower percolation threshold could be expected since as shown in Figure 4.5, the electrical conductivity of Samples A is around 10 times higher than that of Sample B.

From Figure 5.1, it can be found that there is a large scattering in experimental results, which may be caused by the different properties of phase materials, different manufacturing processes, unclear definition of percolation threshold in experimental measurements and inaccurate data of the aspect ratio of CNTs. A clear phenomenon in Figure 5.1 is that on the whole, various experimental percolation thresholds tend to decrease as the aspect ratio of CNTs increases although there are some exceptions. As pointed out in [12], the statistical percolation model may be insufficient to address the inter-particle or the matrix-particle interactions, and a model based on colloid theory may be helpful. In Figure 5.1, however, the theoretical and numerical predictions from the statistical percolation model still pass through the middle area of various scattered experimental data. This result may be reasonable since the traditional percolation model only provides the average possibility of the formation of the first conducting network under the assumption of uniform random distribution of fillers. Obviously, even for traditional electronic composites with carbon short fibers, the experimental results cannot always match the theoretical ones well since the perfect uniform random distribution of carbon short fibers in matrix cannot be always realized practically. Naturally, the extent of scattering in the experimental data of the traditional electronic composites is not as large as that of nanocomposites using CNTs as filler.

Also, in Figure 5.1, an interesting phenomenon in various experimental results is that the percolation thresholds using SWNTs are comparatively higher than the numerical and theoretical values. The reason may be from: difficult dispersion of SWNTs due to easier formation of heavily concentrated aggregates or bundling caused by their much higher absorption energy as shown in Figure 5.2 [35], where the absorbability of SWNTs is around 10 times higher than that of MWNTs. Moreover, generally, there is a lack of uniformity of electrical conductance in SWNTs, which strongly depends on the atomic structural parameters such as the chiral vector. In contrast, the percolation thresholds using MWNTs except that in [19] are lower than the numerical and theoretical ones. The reason may be from the practical small-scale aggregates of MWNTs in the macroscopic conducting network as shown in Figure 4.6(a). In this case, if we consider a chain-like small aggregate formed by MWNTs as a single filler, its effective aspect ratio should be higher than that of one MWNT, which consequently results in the lower percolation thresholds compared with the theoretically predicted value using the original lower aspect ratio of MWNTs. Especially for longer MWNTs, these small aggregates may be formed more easily, it may be a reason of why the results in [10, 11, 12] are much lower than the numerical and theoretical ones.

When CNTs possess L/D and σ_{CNT} as 100 and 10^4 S/m, respectively, the comparison of the present numerical and various experimental results are shown in Figure 5.3. It should be noted that CNTs used in our experiments and in [14, 15] are the same, which are of L/D as 100. This figure demonstrates that the numerical results obtained from the 3D resistor network model agree with the experimental results very well. The influence of curvature of CNTs is insignificant in this case. Again, it confirms the effectiveness of the statistical percolation model for the nanocomposites with MWNTs as filler particles. The main reason can be that the dispersion of MWNTs is comparatively good as shown in Figures. 4.7 and 4.8. Therefore, like the traditional short fiber, each MWNT can be treated as an independent filler particle and the effects of aggregates of MWNTs can be neglected. Naturally, it is further needed to verify the cases of SWNTs as filler particles, since the adsorption energy among SWNTs is much higher than that among MWNTs (around one order higher), which can easily result in the heavily concentrated bundling or aggregates of SWNTs. Also, another issue is about the interactions between CNTs and polymer, such as coating of polymer on CNTs, which has to be considered and reflected in an improved numerical model in the future.

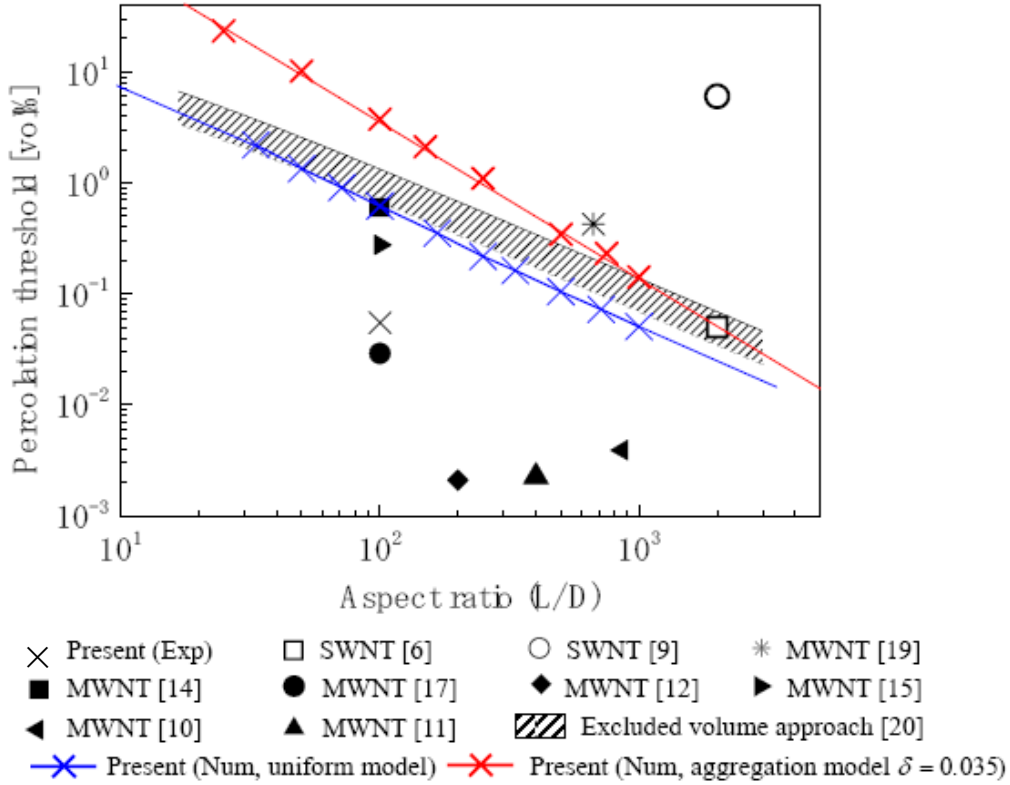


Figure 5.1. Comparison of experimental and numerical results for percolation threshold.

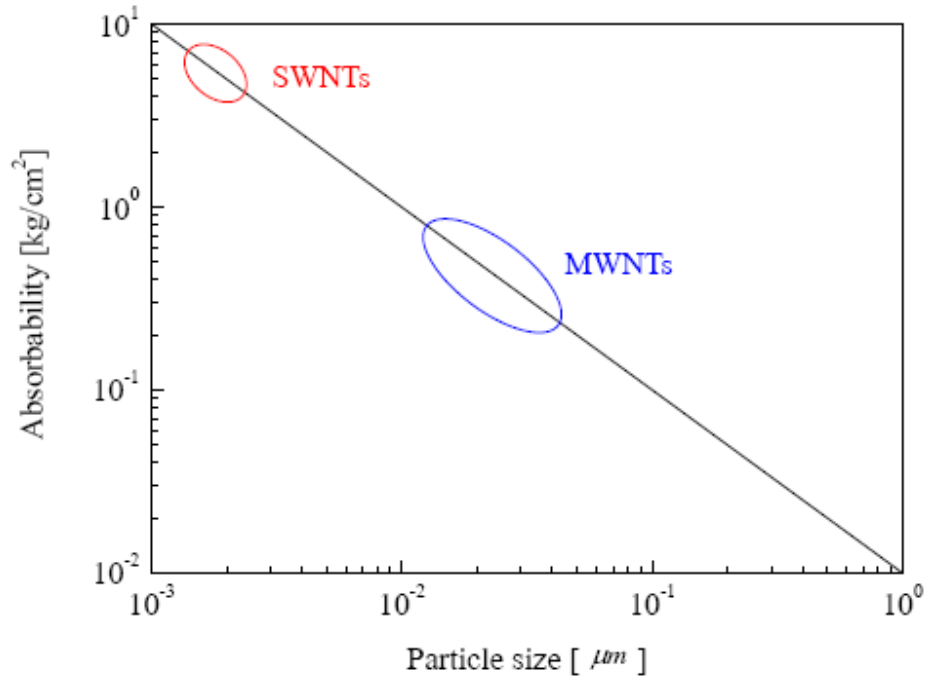


Figure 5.2. Relation between particle size and absorbability by Van der Waals force [35].

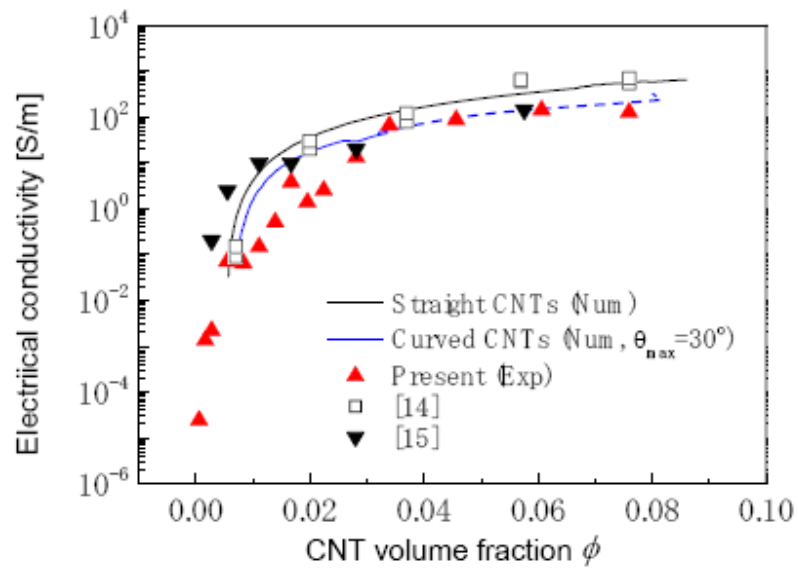


Figure 5.3. Comparison of experimental and numerical results for electrical conductivity.

6. APPLICATION OF NANOCOMPOSITES TO HIGHLY SENSITIVE STRAIN SENSOR

In this section, we will describe a highly sensitive strain sensor, which was developed based on the nanocomposite fabricated previously. The experimentally obtained results indicate that the sensitivity of this new-type sensor is much higher than that of traditional strain gages. Also, an improved numerical model with the consideration of tunnel effect among CNTs will be described and the working mechanism of the sensor will be explored.

6.1. Experiments

By using the fabrication process of Sample B in Section 4, a strain sensor of thickness of around 170 μm was fabricated from this nanocomposite as shown in Figure 6.1. To measure the electrical resistance change of this sensor caused by the prescribed strain, this sensor was attached on the surface of an insulating cantilever beam as shown in Figure 6.2. Also, the traditional strain gage was employed, which was attached on the opposite surface of the beam at the same position of the CNT/polymer sensor. This strain gage was used to measure the strain of the beam at this position. The electrical resistance change of the CNT/polymer sensor was measured using the LCR meter. For the traditional strain gage, the strain is measured from the resistance change of gage caused by its deformation. The gage ratio can be expressed approximately as follows

$$K = \frac{\Delta R/R}{\varepsilon} = \frac{1 + 2\nu - \nu^2 \varepsilon}{(1 - \nu \varepsilon)^2} (\approx 2) \quad (31)$$

where ν is the Poisson's ratio

This equation indicates that the gage ratio of the traditional strain gage is around 2. Also, it should be noted that usually the minimum measurement ability of the traditional strain gage is around 10 $\mu\varepsilon$.

6.2. Numerical Model with Consideration of Tunnel Effect for Resistance Change Caused by Prescribed Strains

Usually, from the results of currently existing studies, the mechanisms of CNT/polymer sensors can be clarified into three aspects: (1) breakup of CNT network due to strain; (2) electrical resistance change of CNTs due to deformation of CNTs; (3) increase of electrical resistance of tunnel effect among CNTs due to the increase of distances among CNTs.

In our study, we only consider the effects of (1) and (3) outlined above. The stretch or compressive deformation in CNTs and the corresponding resistance change of CNTs are neglected due to their much higher Young's modulus than that of epoxy (more than 300 times higher if we take the Young's modulus of CNTs as 1 TPa and the Young's modulus of epoxy as 2.4 GPa). Moreover, in our specimens, the interface between the polymer and CNTs seems

to be weak as shown in Figure 6.3, where a trace of a CNT, which is completely removed from the polymer, is clearly illustrated. The tunnel effect seems to be a very important factor which controls the performance of the CNT/polymer sensor. By seeing Eq. (26), if there is 1

increase of d , i.e., the distance between two CNTs, the tunnel current will be 10 times lower. Especially in the region around the percolation threshold, there are a lot of situations where there are very short distances among CNTs as shown in Figure 3.7. In this case, the electrical charges can still be transferred between two close CNTs without contact, if the distance between them is sufficiently small. When this nanocomposite is under the prescribed strain, we reconstruct our 3D resistor network by considering the rigid-body movement of CNTs in the nanocomposite as shown in Figure 6.4. The changes of position and orientation of CNTs caused by the strain and effect of Poisson's ratio are modeled.

By considering the effects of (1) and (3) outlined above, we have numerically investigated the electrical resistance change of the CNT/polymer sensor under the prescribed strains for the cases of 2.0 wt%, 3.0 wt% and 5.0 wt% of MWNTs loading. From the numerically obtained results, it was found that the electrical resistance change of the sensor is very small if only considering (1), i.e., the breakup of CNT network caused by the strains. The influence of this factor seems to be very tiny at least for small strains under 1% in our numerical simulations. For higher strains, the obtained results may be different. On the other hand, it was found that the tunnel effect leads to the remarkable resistance increase of the sensor under the prescribed strain. It implies that the tunnel effect is a key factor to control the performance of CNT/polymer sensors. However, its effect is limited to a very narrow band around the percolation threshold. It means that the application of this nanocomposite for highly sensitive strain sensor should be focused on the region around percolation threshold.

6.3. Comparison Between Numerical and Experimental Results

The experimental measured results for the resistance change of this new-type sensor is shown in Figure 6.5, where the gage ratio of the traditional strain sensor is $K=2$. The numerical results are shown in Figure 6.6. Both figures show that the sensitivity of this new-type sensor is much higher than that of the strain gage. As the volume fraction of CNTs decreases, which is gradually close to the percolation threshold of the nanocomposite (i.e., 0.1 wt% here), the sensitivity of sensors becomes higher gradually. It verifies our speculations as stated above. Moreover, our numerical results with the consideration of the tunnel effect among CNTs agree very well with the experimental results. Therefore, the modeling of tunnel effect is very important in our numerical simulations. Moreover, it can be concluded that the tunnel effect among CNTs is a key factor for controlling this phenomenon although other factors such as the electrical conductance change of CNTs may also be important (we have not modeled this effect here).

Another interesting phenomenon is that the behavior of resistance change of the CNT/polymer sensor becomes non-linear when the strain is higher as shown in the numerical results in Figure 6.6. For the experimental results shown in Figure 6.5, this non-linear behavior can also be identified although it is not as clear as that in the numerical results. The reason can be found from Eq. (26), where the resistance of tunnel effect depends on the distance between two CNTs in the form of nonlinearity. Due to the existence of this non-

linear behavior, the calibration of this new-type sensor becomes more important and more complex.

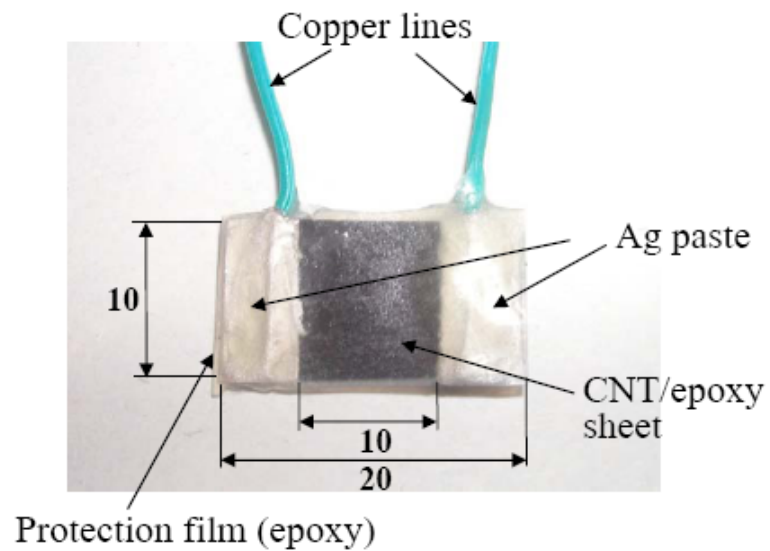


Figure 6.1. Strain sensor fabricated from CNT/polymer nanocomposite.

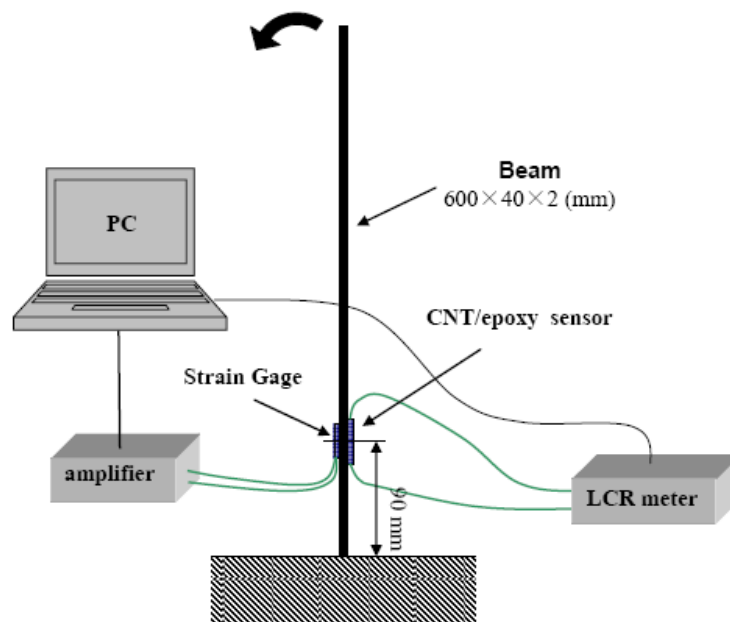


Figure 6.2. Experimental setup for measuring resistance change in strain sensors.

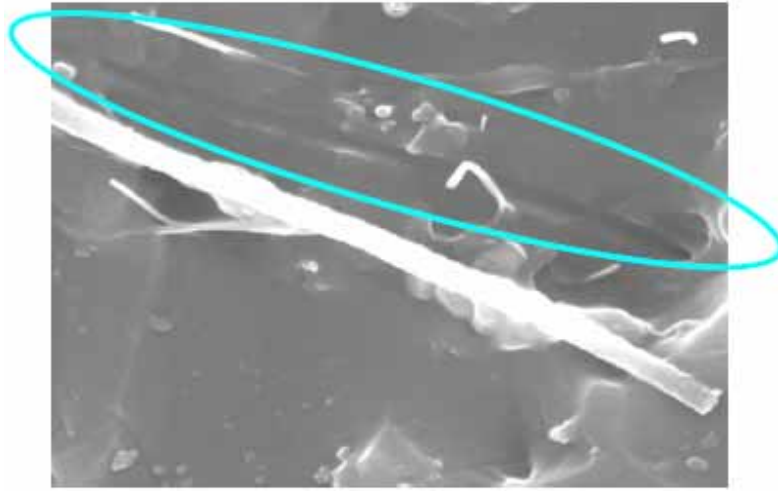


Figure 6.3. A trace of a removed CNT (evidence of weak interface between polymer and CNTs).

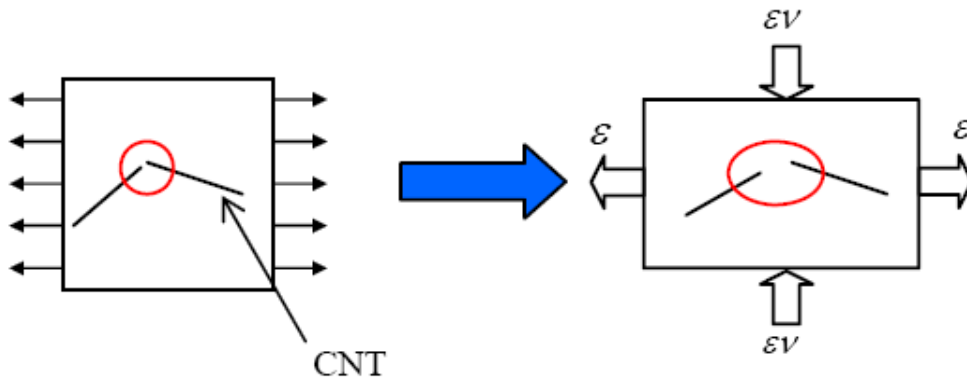


Figure 6.4. Modeling of CNTs movement as rigid-body in sensor.

7. CONCLUSIONS

In this study, the electrical behaviors of a nanocomposite made from an insulating polymer with filled CNTs have been numerically and experimentally investigated. Based on the statistical percolation theory, we proposed a 3D numerical model to predict the electrical properties of the nanocomposite at and after the percolation threshold. In this model, with the assumption of randomly distributed CNTs in the polymer, the percolation threshold was predicted at the volume fraction of CNTs when the first complete electrically-conductive path connected by some CNTs is formed. Furthermore, a 3D resistor network model for electrical conduction problems of composites was proposed to predict the macroscopic electrical conductivity of the nanocomposite after the percolation threshold. The influences of the

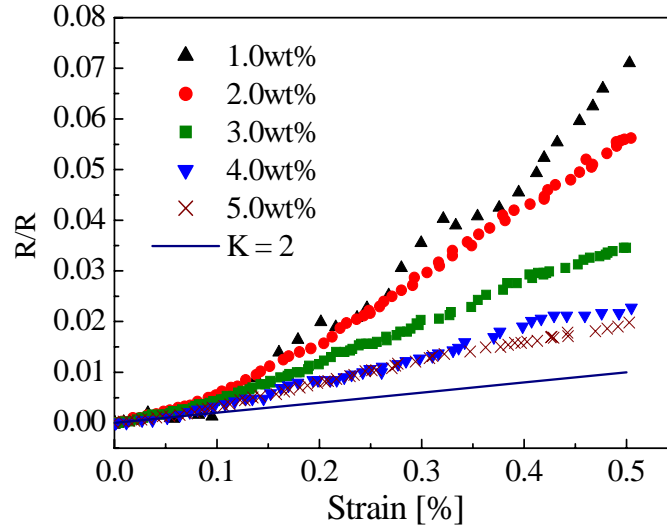


Figure 6.5. Electrical resistance change of CNT/polymer sensor versus strain (experimental results)

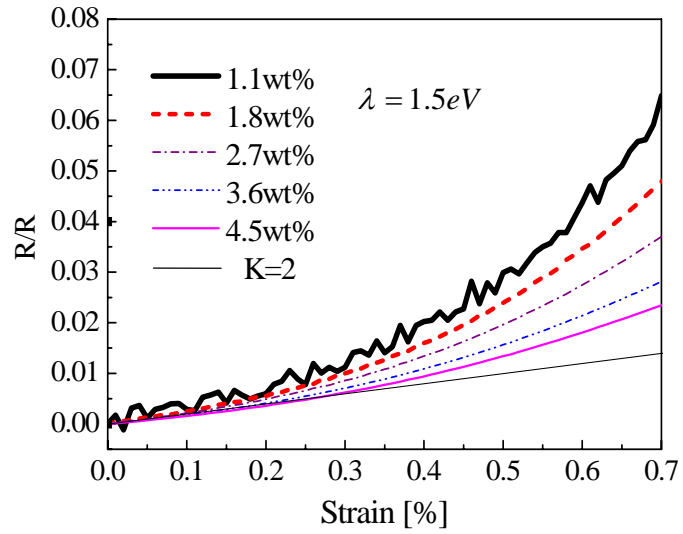


Figure 6.6. Electrical resistance change of CNT/polymer sensor versus strain (numerical results)

shapes of curved CNTs, aggregates of CNTs and the tunnel effect among CNTs have been studied in detail.

In experiments, it was found that the electrical behaviors of the nanocomposite are very complex practically, which strongly depends on the manufacturing process. The different macro-structures of CNTs in the polymer caused by the different fabrication processes are crucial to determine the electrical properties of the nanocomposite. Moreover, the undesirable coating of the polymer on CNTs formed in the manufacturing process may be another key factor controlling the macroscopic electrical performances of the nanocomposite. Although there are a lot of complexities needed to be tackled, based on the traditional statistical percolation theory with some simplifications, the present numerical model for predicting the electrical properties of the nanocomposite was verified to be powerful and effective by comparing the numerical results with the experimental results. The main reason is that the heavily concentrated aggregates of MWNTS are not identified in our experiments. The verified and reliable numerical simulations finally help us obtain a simple empirical formula for predicting the electrical properties of the nanocomposite with sufficient accuracy.

Moreover, a highly sensitive sensor was practically developed from this nanocomposite. Both experimental and numerical results verify its high sensitivity compared with that of the traditional strain gage. When the volume fraction of CNTs is gradually close to the percolation threshold, the sensitivity of this new-type sensor increases gradually. An extended numerical resistor network model by considering the rigid-body movement of CNTs in matrix caused by the strains and the tunnel effect among CNTs is very effective to predict the electrical resistance change of this sensor caused by the strains, which implies that the tunnel effect is a key factor to control the sensor performance.

REFERENCES

- [1] Seo MK, Park SJ. Electrical resistivity and rheological behaviors of carbon nanotubes-filled polypropylene composites. *Chem Phys Lett* 2004; 395(1-3): 44-8.
- [2] Meincke O, Kaempfer D, Weickmann H, Friedrich C, Vathauer M, Warth H. Mechanical properties and electrical conductivity of carbon-nanotube filled polyamide-6 and its blends with acrylonitrile/butadiene/styrene. *Polymer* 2004; 45(3): 739-48.
- [3] Pötschke P, Abdel-Goad M, Alig I, Dudkin S, Lellinger D. Rheological and dielectrical characterization of melt mixed polycarbonate-multiwalled carbon nanotube composites. *Polymer* 2004; 45(26): 8863-70.
- [4] McNally T, Pötschke P, Halley P, Murphy M., Martin D., Bell SEJ, Brennan GP, Bein D, Lemoine P, Quinn JP. Polyethylene multiwalled carbon nanotube composites. *Polymer* 2005; 46(19): 8222-32.
- [5] Nogales A, Broza G, Roslaniec Z, Schulte K, Šícs I, Hsiao BS, Sanz A, García-Gutiérrez, MC, Rueda DR, Domingo C, Ezquerro TA. Low Percolation threshold in nanocomposites based on oxidized single wall carbon nanotubes and poly(butylene terephthalate). *Macromolecules* 2004; 37(20): 7669-72.
- [6] Ounaies Z, Park C, Wise KE, Siochi EJ, Harrison JS. Electrical properties of single wall carbon nanotube reinforced polyimide composites. *Compos Sci Technol* 2003; 63(11): 1637-46.

-
- [7] Park C, Wilkinson J, Banda S, Ounaies Z, Wise KE, Sauti G, Lillehei, PT, Harrison JS. Aligned single wall carbon nanotube polymer composites using an electric field. *J Polym Sci, Part B: Polym Phys* 2006; 44(12): 1751-62.
 - [8] Kymakis E, Alexandou I, Amaratunga GAJ. Single-walled carbon nanotube-polymer composites: electrical, optical and structural investigation. *Synthetic Metals* 2002; 127(1-3): 59-62.
 - [9] Kymakis E, Amaratunga GAJ. Electrical properties of single-wall carbon nanotube-polymer composite films. *J Appl Phys* 2006; 99: 084302.
 - [10] Sandler J, Shaffer MSP, Prasse T, Bauhofer W, Schulte K, Windle AH. Development of a dispersion process for carbon nanotubes in an epoxy matrix and the resulting electrical properties. *Polymer* 1999; 40(21): 5967-71.
 - [11] Sandler JKW, Kirk JE, Kinloch IA, Shaffer MSP, Windle AH. Ultra-low electrical percolation threshold in carbon-nanotube-epoxy composites. *Polymer* 2003; 44(17): 5893-9.
 - [12] Martin A, Sandler JKW, Shaffer MSP, Schwarz MK, Bauhofer K, Schulte K, Windle AH. Formation of percolating networks in multi-wall carbon-nanotube-epoxy composites. *Compos Sci Technol* 2004; 64(15): 2309-16.
 - [13] Ogasawara T, Ishida Y, Ishikawa T., Yokoda R. Characterization of multi-walled carbon nanotube/phenylethynyl terminated polyimide composites. *Composites: Part A* 2004; 35(1): 35-67.
 - [14] Ono U, Aoki T, Ogasawara T. Mechanical and electrical properties of MWNT reinforced composites. *Proc. of the 48th Conference on Structural Strength in Japan*, July 2006, Kobe, 141-3 (in Japanese).
 - [15] Research Report, Nano Carbon Technologies Co., Ltd, 66-2 Horikawamachi, Saiwai-ku, Kawasaki shi, Kanazawa, 2004 (private communication)
 - [16] Jiang X, Bin Y, Matsuo M. Electrical and mechanical properties of polyimide-carbon nanotubes composites fabricated by in situ polymerization. *Polymer* 2005; 46(18): 7418-24.
 - [17] Kilbride EB, Coleman JN, Fraysse J, Fournet P, Cadek M, Drury A, Hutzler S, Roth S, Blau WJ. Experimental observation of scaling laws for alternating current and direct current conductivity in polymer-carbon nanotube composite thin films. *J. Appl. Phys.* 2002; 92(7): 4024-30.
 - [18] Du F, Fisher JE, Winey KI. A coagulation method to prepare single-walled carbon nanotube/PMMA composites and their modulus, electrical conductivity and thermal stability. *J Polym Sci, Part B: Polym Phys* 2003; 41(24): 3333-8.
 - [19] Hu G, Zhao C, Zhang S, Yang M, Wang Z. Low percolation thresholds of electrical conductivity and rheology in poly(ethylene terephthalate) through the networks of multi-walled carbon nanotubes. *Polymer* 2006; 47(1): 480-8.
 - [20] Celzard A, McRae E, Deleuze C, Dufort M, Furdin G, Marêché JF. Critical concentration on percolating systems containing a high-aspect-ratio filler. *Phys. Rev. B* 1996; 53: 6209-14.
 - [21] Balberg I, Anderson CH, Alexander A, Wagner N. Excluded and its relation to the onset of percolation. *Phys. Rev. B* 1984; 30: 3933-43.
 - [22] Balberg I, Binenbaum N. Cluster structure and conductivity of three-dimensional continuum systems. *Phys. Rev. A* 1985; 31: 1222-5.

-
- [23] Newman MEJ, Ziff RM. Fast Monte Carlo algorithm for site or bond percolation. *Phys. Rev. E* 2001; 64: 016706.
 - [24] Kirkpatrick S. Classical transport in disordered media: scaling and effective-medium theories. *Phys. Rev. Lett.* 1971; 20: 1722-5.
 - [25] Kirkpatrick S. Percolation and conduction. *Rev. Mod. Phys.* 1973; 45: 574-88.
 - [26] Thess A, Lee R, Nikolaev P, Dai H, Petit P, Robert J, Xu C, Lee YH, Kim SG, Rinzler AG, Colbert DT, Scuseria GE, Tomanek D, Fischer JE, Smalley RE. Crystalline ropes of metallic carbon nanotubes. *Science* 1996; 273: 483-7.
 - [27] Ebbesen TW, Lezec HJ, Hiura H, Bennett JW, Ghaemi HF, Thio T. Electrical conductivity of individual carbon nanotubes. *Nature* 1996; 382: 54-6.
 - [28] Fischer JE, Dai H, Thess A, Lee R, Hanjani NM, Dehaas DL, Smalley RE. Metallic resistivity in crystalline ropes of single-wall carbon nanotubes. *Phys. Rev. B* 1997; 55: R4921-4.
 - [29] de Heer WA, Bacsá WS, Châtelain A, Gerfin T, Humphrey-Baker R, Forro L, Ugarte D. Aligned carbon nanotube films: production and optical and electronic properties. *Science* 1995; 268: 845-7.
 - [30] Hobara R, Yoshimoto S, Ikuno T, Katayama M, Yamauchi N, Wongwiriyan W, Honda S, Matsuda I, Hasegawa S, Oura K. Electronic transport in multiwalled carbon nanotubes contacted with patterned electrodes. *Jpn J Appl Phys* 2004; 43: L1081-4.
 - [31] Deutscher G. Disordered systems and localization. in *Percolation and Superconductivity*, ed. by A.M. Goldman and S.A. Wolf, Plenum Press, New York, 95-113, 1984
 - [32] Stauffer D. *Introduction to Percolation Theory*, Taylor and Francis, London, 1985.
 - [33] Simmons JG. Generalized formula for the electric tunnel effect between similar electrodes separated by a thin insulating film. *J. Appl. Phys.* 1963; 34: 1793-1803.
 - [34] Kang I, Schulz MJ, Kim JH, Shanov V, Shi D. A carbon nanotube strain sensor for structural health monitoring. *Smart Mat. Struct.* 2006; 15: 737-48.
 - [35] Kondo T, Suzuki S. *Introduction of Colloid Theory and Interface Science*. Sankyo Press, Tokyo, 2000 (in Japanese).